# Circular Polarized Light Emission in Chiral Inorganic Nanomaterials

Shuang Jiang a,b Nicholas A. Kotov b,\*

[a] S. Jiang,

Tianjin Key Laboratory of Applied Catalysis Science and Technology, School of Chemical Engineering and Technology, Tianjin University, No. 135, Yaguan Road, Tianjin 300350, P. R. China

[b] N. A. Kotov,

Department of Chemical Engineering, Biointerfaces Institute, Department of Materials Science and Engineering, Department of Biomedical Engineering and Department of Mechanical Engineering, University of Michigan, Ann Arbor, Michigan 48109, United States

\* Corresponding author: kotov@umich.edu.

ABSTRACT: Chiral inorganic nanostructures strongly interact with photons changing their polarization state. The resulting circularly polarized light emission (CPLE) has cross-disciplinary importance for a variety of chemical/biological processes and is essential for development of chiral photonics. However, the polarization effects are often complex and could be misinterpreted. CPLE in nanostructured media has multiple origins and several optical effects are typically convoluted into a single output. Analysing CPLE data obtained for nanoclusters, NPs, nanoassemblies, and nanocomposites from metals, chalcogenides, perovskite, and other nanostructures, we show that there are several distinct groups of nanomaterials for which CPLE is dominated either by circularly polarized luminescence (CPL) or circularly polarized scattering (CPS); there are also many nanomaterials for which they are comparable. We also show that (1) CPL and CPS contributions involve light-matter interactions at different structural levels; (2) contribution from CPS is especially strong for nanostructured microparticles, nanoassemblies and composites; and (3) engineering of materials with strongly polarized light emission requires synergistic implementation of CPL and CPS effects. These findings are expected to guide development of CPLE materials in a variety of technological fields, including 3D displays, information storage, biosensors, optical spintronics, and biological probes.

**Keywords:** chiral nanostructures, photonics, mirror asymmetry, nanoparticles, scattering, nanocomposites.

#### 1. INTRODUCTION

Materials with strong stimulated circular polarized light emission (CPLE) have attracted increased attention over the last decade due to the significance of circular polarization as a carrier of biological/chemical information and as a photonic effect essential for optoelectronic devices. Concomitantly, a wide variety of chiral nanostructures has been synthesized, opening a new toolbox to produce CPLE with various intensities, photon energies, and degrees of polarization. Attaining simultaneously high ellipticity and intensity of emitted photons in a specific spectral window with specific wavelength maximum and width, is a challenging task. Besides experimental intuition, it requires careful analysis and deciphering the complexity of optical processes taking place in chiral nanomaterials, which represents the goal of this review.

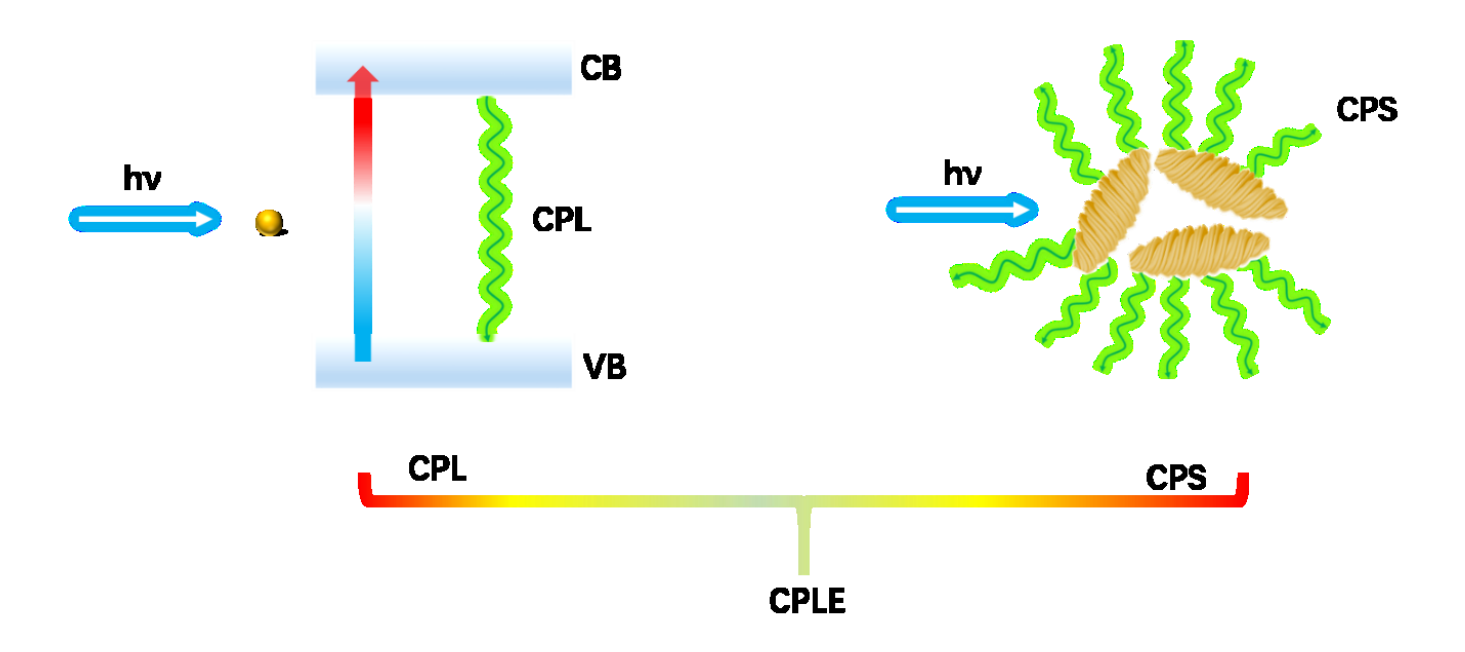
## 1.1. Light-matter interactions contributing to CPLE

When light passes through luminescent chiral medium containing nanoscale components, both circularly polarized luminescence (CPL) and circularly polarized scattering (CPS, also known as differential scattering) can occur. We will use the term CPLE referring to the polarized net flux of photons leaving the optically active media that carry the cumulative effects of both CPL and CPS, (Scheme 1).

<u>Circularly polarized luminescence</u>. Circularly polarized emission associated with CPL originates from luminescent or phosphorescent quantum states of chiral nanostructures or molecules dispersed in the media. Considering the mechanism of CPL generation, a photon emitted from a chiral excited state acquires polarization because of non-zero dot product between the electric dipole transition moment and the imaginary magnetic dipole transition moment characterizing the electronic transition responsible for luminescence. A number of excellent studies about CPL in small organic molecules, metal organic complexes, and their thin films have been published.<sup>[1-4]</sup> Here we focus on the physics of CPL in nanoclusters, nanoparticles (NPs), nanoassemblies, and nanocomposites that are commonly used now as CPLE-active materials.

<u>Circularly polarized scattering</u>. Once emitted, the photon must pass through the chiral media. When solutions and thin films of chiral compounds are typically assumed to be optically homogenous at the molecular level (i.e., at the level much below the wavelength of visible light), one can typically ignore scattering for most of the organic/inorganic molecules and polymeric materials studied in the past. However, this is no longer the case for nanoscale structures, which can absorb and scatter light simultaneously giving rise to both CPL and CPS. Additional complexity can also emerge from self-organization that is an innate property of NPs and other nanomaterials.<sup>[5]</sup>

The term CPS will refer to the light-matter interactions with nanostructures resulting in predominant scattering of either left- or right-circularly polarized light (Scheme 1). Unlike CPL, the wavelength, intensity and ellipticity of photons produced by CPS depends strongly on the shape, chirality, and orientation of the emitting particle. Compared to molecules and small inorganic clusters with dimensions much smaller than the wavelength of light, CPS becomes increasingly important and its contribution to CPLE and other optical phenomena increases with the NP size. Dispersions of relatively small NPs with diameters much smaller than the wavelength of incident light (20-50 nm) produce Raleigh scattering with circular polarization dependent on geometrical shape and mirror asymmetry of the optical constants of the inorganic lattice comprising the NPs. The intensity of Raleigh scattering is proportional to  $(R/\lambda)^4$ , where R and  $\lambda$  are the radius of irradiated nanomaterial and the wavelength of the scattered light, respectively and has no strong angular dependence of the emitted light.



Scheme 1. The schematic illustration of the physical mechanism of CPL (left) and CPS (right).

Nanostructured particles with at least one dimension larger than 100 nm produce Mie scattering.<sup>[8, 9]</sup> The circular polarization of Mie scattering is linearly proportional to the chirality parameter,  $\kappa$ , of the nanomaterial, where  $\kappa$  characterizes the strength of the cross-coupling between the magnetic and electric fields.<sup>[10-12]</sup> Chiral plasmonic nanomaterials are particularly common and almost always display strong Mie scattering.<sup>[8]</sup> Both absorption and scattering of light with frequency  $\omega$  by

plasmonic NPs reaches maxima when  $\lambda$  lies in the vicinity of the particle's surface plasmon resonance frequency,  $\lambda_{plasmon}$ . Formation of assembled structures where plasmonic NPs produce interparticle resonances can increase ellipticity and intensity of CPS while making possible its 'tuning' across different wavelengths. The same effect is also used in optical metamaterials where Mie scattering from individual scatterers can also experience interference further enhancing the desired effects. Besides well-known metals with  $\lambda_{plasmon}$  in the visible range (predominantly gold and silver), plasmonic effects from some high-index dielectric nanomaterials are also measurable. [10]

Another important case of CPS includes periodic variations of refractive index resulting in the Bragg-like scattering of photons. When the material is chiral and periodic, the light passing through such optical media may acquire circular polarization due to allowed and forbidden photonic states. Transparency of the material becomes dependent on the helicity of the photon when the periodically placed scatterers are chiral and the structural repeating unit has characteristic scale comparable with the wavelength of light. These materials can also be described using the notion of photonic bandgap that becomes polarization-dependent. [14, 15] For example, the left-handed photons can be selectively reflected and scattered in the right-handed colloidal crystals and vice versa, leading to the selective transmission of right-handed photons. [14-16] Some of such materials are well known and include chiral liquid crystal or cholesteric structures that generate CPLE arising from CPS while being emitted from achiral emitters. [14, 16]

<u>CPLE-active materials.</u> Both CPL and CPS may play important roles in modulation of circular polarization of photons and have a strong impact on CPLE. In general, both of these contributions need to be analyzed in concert to avoid misattribution and misinterpretation of the light-matter interactions that can occur in nanostructured optical media. For example, asymmetry of molecular orbitals or other quantum states involved in the excited-to-ground state transition cannot explain ellipticity of emitted light in many experimental cases. [16-18] Moreover, the photons emitted from excited states as a result of CPL may have no ellipticity but acquire circular polarization as a result of CPS. [17] Similarly, the circular polarization of photons emitted from the chiral quantum states as a result of CPL can change sign after CPS. Intensity and directionality of CPLE are also strongly affected by CPS on dispersed particles with nanoscale, submicrometer-scale, or micrometer-scale chirality, which can be both beneficial to the intended function of the material or not.

The overarching question now is how to differentiate the contributions of CPS and CPL. This problem has yet to be resolved for many cases of nanostructured optical media. Not only chemistry of specific nanostructures, but preparation of the samples, and, in particular thin films, can strongly

change the relative contributions of CPL and CPS. In some cases, one of them dominates and is sufficient to rationalize CPLE. These are several cases where either the contribution of CPL or CPS dominates and the physical picture of the light-matter interactions can be simplified:

- (1) small NPs with chiral quantum states and diameters much below the wavelength of the emitted photon;
- (2) large nanostructured particles with chiral features such as pitch, with dimensions comparable to the wavelength of the emitted photon;
- (3) plasmonic nanomaterials when  $\lambda \rightarrow \lambda_{\text{plasmon}};^{[19, 20]}$
- (4) extended nanostructures and photonic nanocomposites with periodicity comparable to the  $\lambda$ .

Barring some of the nonlinear processes such as second order Raleigh scattering and circularly polarized Mie scattering, [10, 21] CPLE can be attributed solely to CPL for the first case of NPs that are uniformly dispersed in optically homogeneous media. Such materials include organic complexes, metallic nanoclusters, nanoscale semiconductors, and nanostructured perovskites. CPLE has the dominant contribution from CPS for the second, third, and fourth cases regardless of the sample preparation methods. Even if the dispersion is visibly transparent as the case with many plasmonic particles, scattering processes should be considered when interpreting the origin of photon ellipticity.

In the subsequent sections, we will review the studies of CPLE in nanostructures according to these cases focusing specifically on the family of nanomaterials with CPL- and CPS-dominant circular polarization (Sections 2 and 3, respectively). There are also many cases where the contributions of CPL and CPS are comparable and interdigitated. These cases are interesting and important but making a definitive judgement about the origin of ellipticity in light emission for these experimental systems is often difficult based on the existing data. Note also that the mechanisms can be strongly dependent on the wavelengths of the photons passing through the CPLE-active material. Both experimental and modeling studies are needed to correctly interpret optical events taking place in such media.

<u>1.2. Metrology</u> While the physical natures of CPL and CPS are different, the same instrumentation and metrics can be applied to enumerate the outcome of both optical processes. As such, the degree of CPLE polarization can be quantified by the *optical dissymmetry factor* g<sub>CPLE</sub>:

$$g_{CPLE} = \frac{I_L - I_R}{1/2(I_L + I_R)} = \frac{\Delta I}{I}$$
 (1)

where  $I_L$  and  $I_R$  stand for the intensity of left- and right-polarized emission measured separately.  $g_{CPLE}$  is mathematically identical to  $g_{lum}$  often reported in CPL studies but reflects greater diversity of optical processes contributing to polarization rotation than just luminescence. The measurements of  $g_{CPLE}$  are typically carried out by circularly polarized luminescence spectrometer and in the case of CPL-dominant materials, the  $g_{CPLE} \approx g_{CPL} \equiv g_{lum}$ . Note that the light incident onto the sample in CPL measurements is unpolarized and the CPL spectra return the degree of polarization of the emitted light. Intensity of the left- and right-polarized emission enable one to calculate  $g_{CPLE}$  according to Eq. (1). Other optical techniques evaluating CPLE when the incident light is circularly polarized can also be used, but they are less common.

The same instrumentation can be applied to study CPS-dominant materials, but  $g_{CPLE}$  describes circular polarization acquired because of scattering. One can certainly introduce two separate notations  $g_{CPS}$  and  $g_{CPL}$ , but it will make the discussion unnecessarily complicated and, at times, confusing. Furthermore, CPLE spectra may contain both CPL- and CPS-dominant peaks depending on the wavelength. For example, Mie scattering peaks from gold NPs are localized in the red-part part of the CPLE spectrum, while CPL peaks from chiral ligands on their surface are often localized in its blue part. Thus, the use of  $g_{CPLE}$  as a unifying measure of polarization for emitted light regardless of the nature of light-matter interactions, is advocated for strongly scattering nanostructures. It also gives a convenient cumulative characteristic relevant for practice and subsequent utilization of CPLE-active nanomaterials.

Similarly to  $g_{lum}$ , the values of  $g_{CPLE}$  can vary between -2 and 2. When it is 0, the emission is unpolarized. The maximum values of 2 or -2 respectively means that the light is completely left- or right-polarized. In most cases in this article, we will use the absolute value of  $|g_{CPLE}|$  because of the reciprocity relationships with the chirality of emitters. Switching the handedness of the emitter to its opposite results in the change of sign of  $g_{CPLE}$ . The absolute value is also most relevant from a technical standpoint. We note that it is quite difficult to achieve  $|g_{CPLE}|$  values above 1.0. The typical values of  $|g_{CPLE}|$  for small molecules and many nanostructures are between  $10^{-4}$  and  $10^{-2}$ . The best-known CPL-active materials, chiral lanthanide complexes, display some of the highest  $|g_{CPLE}|$  values with a typical range between 0.05 and 0.5. The highest values of CPL-dominant CPLE with  $|g_{CPLE}| = 1.38$  were obtained for cesium tetrakis(3-heptafluoro-butylryl-(+)-camphorato)Eu(III) complexes in EtOH and CHCl<sub>3</sub> solutions, [22] but at the expense of total photon flux. The strong polarization rotation of the emitted photons in this case is due to luminesce from hybrid excited states involving the atomic orbitals of metals and chiral organic ligands. [23-25] Despite high values of optical asymmetry, their intensity is low, which reflects the fundamental contrarian

relationship between the degree of polarization and intensity of emission imbedded in the proportionality of  $g_{lum}$  to the dot product between the transient electric and imaginary magnetic dipole moments. Consequently, chiral molecules with strong luminescence typically display optical asymmetry factors below  $10^{-3}$ . Also, the emission of many chiral organic substances fades with time, which greatly restricts CPL application. Utilization of chiral nanostructures and careful engineering of their structure opens the path to resolution of this contrarian relationship. Inorganic nature of the NPs, their assemblies, and photonic nanocomposites also increases the stability of CPLE-active materials to environmental factors and photo-oxidation.

## 2. Nanomaterials with Luminescence-Dominant Circularly Polarized Light Emission

The CPLE for dispersions of nanoclusters or NPs are CPL-dominant because the emitters are too small to cause sufficiently strong Mie and Raleigh effects in the part of the spectrum being used for CPLE measurements, which is typically the visible range. This type of optical media is transparent, and NPs are uniformly dispersed in the liquid solvents or thin films. The CD and CPLE data from solidified and dried films of CPL-active nanostructures should be considered with care because they are often optically anisotropic due to intrinsic self-assembly,<sup>[5]</sup> that may cause linear dichroism and circular birefringence. It is advisable that the polarization effects in thin films be analyzed by Muller matrix polarimetry.<sup>[26]</sup>

#### 2.1 CPLE from chiral metallic nanoclusters

Let us now consider typical examples of CPL-dominant nanomaterials. Noble metal nanoclusters (<2 nm, <200 atoms) have photoluminescence (PL) due to the quantum size effect and splitting of the overlapping populated and unpopulated states into discrete electronic states. <sup>[27, 28]</sup> Nakashima et al. employed R/S- $\alpha$ -dihydrolipoic acid (DHLA) ligands to synthesize Ag<sub>29</sub>(R/S-DHLA)<sub>12</sub> nanoclusters that were the first examples of metallic nanoclusters demonstrating CPLE activity. DHLA ligands are attached as 'staples' to the metal core resulting in the chiral excited states <sup>[29]</sup> leading to CD and CPLE activity with the highest  $|g_{CPLE}|$  value of  $2\times10^{-3}$ . <sup>[29]</sup> The bimetallic nanoclusters, Ag<sub>24</sub>Au<sub>1</sub>(R/S-BINAS)<sub>x</sub>(DMBT)<sub>18-2x</sub> where R/S-BINAS is R/S-1,1'-[binaphthalene]-2,2'-dithiol, DMBT = 2,4-dimethylbenzenethiolate) and x = 1-7 were synthesized by Krishnadas et al. <sup>[30]</sup> As the number of BINAS ligands increases, the low-energy electronic transitions go from achiral to chiral and back to achiral for pure Ag<sub>24</sub>Au<sub>1</sub>(DMBT)<sub>18</sub> to Ag<sub>24</sub>Au<sub>1</sub>(R/S-BINAS)<sub>x</sub>(DMBT)<sub>18-2x</sub>. The  $|g_{CPLE}|$  values for Ag<sub>24</sub>Au<sub>1</sub>(R/S-BINAS)<sub>x</sub>(DMBT)<sub>18-2x</sub> nanoclusters (x = 0~5) are relatively low, around  $1.5\times10^{-4}$ . The computational data indicate that the PL in Ag<sub>24</sub>Au<sub>1</sub>(DMBT)<sub>18</sub> originates from the transitions involving the whole Ag<sub>24</sub>Au<sub>1</sub>S<sub>18</sub> framework, not only from the Ag<sub>12</sub>Au<sub>1</sub> core. <sup>[30]</sup> To the best of our knowledge, Au nanoclusters with CPLE activity

have not been reported, but are certainly possible because small Au NPs and nanoclusters have distinct green luminescence with relatively high photoluminescence quantum yield.<sup>[31, 32]</sup> CPLE-active nanomaterials based on Au and Ag metallic nanoclusters can also be attained, with their activity mainly due to the CPS, which will be discussed in *Section 3*.<sup>[33, 34]</sup>

### 2.2. CPLE from Nanocarbons

The chirality of carbon-based nanomaterials can originate from their basic chemical structure (e.g., the twist in nanotubes) or imparted through chemical modification with chiral ligands. [35, 36] While many CD-active nanocarbon materials have been demonstrated that they typically do not reveal any circular polarization for emitted photons. [35-39] In fact, nanocarbons have quite fascinating emission characteristics defying the rules established for other nanostructures. [40] The fairly strong CPLE was observed for chiral sidewall segments of (-)/(+)-(12,4) carbon nanotubes with the height of ca. 1 nm and diameter of ca. 0.68 nm obtained by separation with chiral high performance liquid chromatography. [41] Their |gcPLE| was reported to be as high as 0.1 - some of the highest values for nanostructures. In these cases, CPLE originates from the PL from electronic states produced by conjugated chiral macrocycles. Note that these types of nanostructures have distinct similarities with similar CPL-active molecules based on condensed aromatic rings [42, 43] exemplified by helicenes. [44-46] With high confidence, one can attribute the emission of circularly polarized photons in the chiral sidewall segments of carbon nanotubes to the strongly delocalized states that have helical shapes determined by the rigid geometry of their aromatic rings.

### 2.3 CPLE from chiral semiconductor NPs

NPs of CdSe, CdS, CdTe, ZnS, ZnO and other semiconductor materials can carry chiral ligands transferring chirality to the inorganic core. Most often these surface ligands are amino acids that may have multiple points of attachment to the semiconductor crystal lattice. The chirality of amino acids makes these NPs CD-active (unless the surface ligands are present as racemates) but the majority of them are CPLE-silent despite the fact that they have sufficiently high PLQY. Several structural and electronic requirements are needed to produce CPL that can originate from both excitonic states associated with the inorganic cores and the hybridized states on the surfaces of NPs. Accurate account of light-matter interactions of CPL-dominant NPs also requires consideration of the chirality of the semiconductor core that can manifest in different forms: the particle shape overall; chiral crystal lattice; chiral light-emitting surface states; chiral defects; and potentially others. One of the most common mechanisms of CPL in semiconductor NPs is via hybridization

of the molecular orbitals of surface ligands with surface-localized electronic states of the NPs. [47, 48] However, the PLQY of the surface states in NPs is often low due to rapid electron-hole recombination processes. Perhaps the best pathway to CPL with high intensity and strong polarization asymmetry is the chiral excitons that can emerge due to the chirality of the crystal lattices of the semiconductor materials. Some semiconductors can crystallize into atomic lattices belonging to mirror asymmetric point groups naturally. For others, the atomic scale chirality can originate from the chiral distortions caused by the organic ligands on NP surface or templates the nanostructures are adhering to. For example, the chiral distortions caused by organic ligands are common in perovskite materials (Section 2.4). Another possibility is the hybridization of the surface states with excitons that can occur, for instance, in small NPs or nanoclusters with butterfly bridging of the orbitals. [49]

The first CPLE-active individual semiconductor NPs were reported by Naito et al. in 2010. [25] CdS NPs with an average diameter of 7.1 nm were synthesized inside a chiral 'cage' template of horse spleen ferritin (**Figure 1a-b**). Two left-handed positive CPLE peaks at 498 and 780 nm appear, arising from the excitonic transition of the CdS core and emission from the surface sites, respectively. UV illumination lamp at 310 nm results in reduction of the NP size from 7.1 nm to 6.0 nm and concomitant blue-shift of the surface state peak by 43 nm. The CPL-active excitonic band, however, disappeared, and CPLE activity became solely reliant on the luminescence from the surface states. The values of  $|g_{CPLE}|$  in these chiral biomimetic nanostructures do not exceed  $8.0 \times 10^{-3}$  [25]

Based on the mechanisms of CPL-dominated emission, one might expect that CPLE from these NPs can be regulated through the chiral ligand concentration or the morphology of metal chalcogenides forming the NP core. Actually, it is even more convoluted than one could expect from the interpretation of CPLE based exclusively on CPL. For example, amino acid-stabilized CdSe, CdS, CdTe, and ZnS NPs with different morphologies were synthesized, whose chiral geometry were usually induced by cysteine and penicillamine. [25, 47, 50] Balaz et al [51] reported the CPL from CdSe NPs with an average size of 2.9 nm and  $|g_{CPLE}|$  of  $(3\sim4)\times10^{-3}$  (Figure 1c-e). [52] These NPs acquired chirality through the process of ligand exchange by extracting NPs stabilized by 'fatty' hydrophobic ligands into the aqueous phase containing L- or D-cysteine. Compared to the direct synthesis of chiral NPs and nanoclusters, the chirality transfer via ligand exchange is more prone to accumulation of electron and hole traps because the NP surface made in the presence of hydrophobic ligands, such as TOPO, is not identical to that made in the presence of L- or D-

cysteine. The mismatch leads to the additional mid-bandgap states activating non-radiative recombination, thus muting the CPLE activity.

One may hypothesize that this quenching can be partially avoided by coating CdSe with a thin layer of CdS.<sup>[52]</sup> The additional shell from a wide band gap semiconductor that is typically added to increase photoluminescence quantum yield, also reduces the chirality transfer from amino acid ligands to the PL-active core. As was demonstrated for 3-8 nm CdSe NPs and nanorods coated with CdS, *g*-factors decreased by an order of magnitude as the thickness of the shell increased (**Figure 1f-g**). Somewhat counterintuitive, an increase of the concentration of the chiral ligand decreased |*gcple*| of CdS-coated CdSe nanorods. As the ratio of cysteine to nanorods increased from 10k, to 20k, 50k, 100k, and 200k, the |*gcple*| values dropped from 3.4/3.9×10<sup>-4</sup> to 1.8/2.5×10<sup>-4</sup>. The CPLE trend is also consistent with that observed in CD peak intensity, indicating the fundamental inhibition of the asymmetry of the light-emitting states.<sup>[52]</sup> Although the quantum mechanical mechanism of this effect may require further investigation, this trend clearly shows the significance of (1) surface states in the chiroptical activity of these semiconductor nanostructures and (2) geometrical + chemical match between the atomic structure of the NP core and the chiral surface ligands.

J. Hao et al. investigated CPLE-active CdSe/CdS nanostructures with different morphologies, such as long rods, short rods, and tadpoles. CPLE intensity in these dispersions exhibits an inverse dependency on the CdS shell thickness and proportionality to the photoluminescence quantum yield. Among these nanostructures, the smallest rods with diameters of 3.2 nm and lengths of 8.7 nm show the highest  $|g_{CPLE}|$  of  $8.5 \times 10^{-4}$ . For the tadpole-shaped particles with lengths from 22.5 nm to 180.8 nm, CPS must be considered due their increased physical dimensions. Attempting to integrate the core-shell PL-enhancement of structures with efficient chirality transfer, CdSe nanoplatelets with lateral sizes of around  $25 \times 5$  nm<sup>2</sup> capped by L-/D-cysteine with island-like CdS shells were synthesized achieving the maximum  $|g_{CPLE}|$  of  $5.29 \times 10^{-4}$ , which indicates that optimization of CPLE optical asymmetry from nanocolloids is likely to require a conceptual change of the chirality transfer protocol.

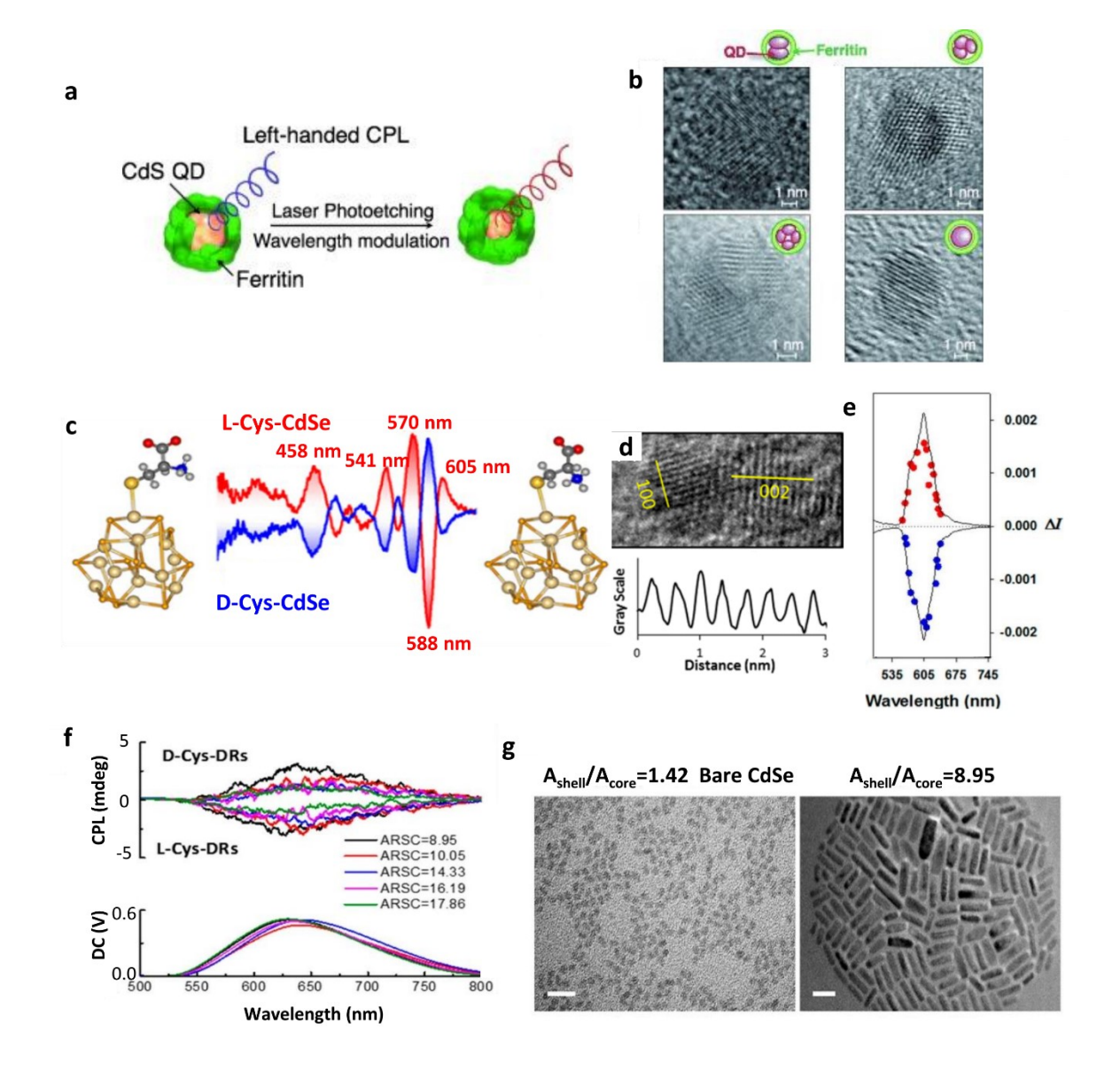


**Figure 1** CPLE from chiral semiconductor NPs capped with chiral ligands. (a) CdS NPs prepared in ferritin and CPLE before and after laser photoetching. (b) HRTEM images of CdS NPs inside ferritin cage containing two, three, four, and one NPs. (c) Structure of chiral nanoclusters of CdSe capped by *L/D*-cysteine. (d) HRTEM image and (e) CPL spectra of chiral CdSe NPs. (f) The CPL spectra and (g) typical TEM images of the *L-/D*-Cys-CdSe/CdS core/shell structure with different values of the absorption ratio of the shell to the core. The TEM scale bar is 20 nm. ARSC in (f) is short for the absorption ratio of shell to core. (a)-(b) Reproduced with permission. [25] Copyright 2010, Wiley-VCH. (c)-(e) Reproduced with permission. [51] Copyright 2013, American Chemical Society. (f)-(g) Reproduced with permission. [52] Copyright 2018, American Chemical Society

# 2.4 CPLE from chiral perovskites

Perovskite nanostructures based on MeX<sub>6</sub> octahedrons, where Me is a transition metal atom and X are oxygen or halogen atoms, attracted a lot of interest from researchers because of their relatively low cost, high defect tolerance, simple synthesis, diversity of structural components, and novelty of optical, electric, and magnetic properties.<sup>[55, 56]</sup> Despite a long history of macroscale perovskite crystals with mirror asymmetry,<sup>[57]</sup> the nanoscale versions of chiral perovskites represent a new development in this field.<sup>[58]</sup> Although many chiral perovskite nanomaterials display strong CD spectra, not all of them are CPLE active,<sup>[59-61]</sup> which depends on the efficiency of chirality transfer, specifics of the emitting quantum states, and the size of the nanostructures.

Chirality transfer in perovskite nanostructures. Similar to many nanocarbons and semiconductor NPs considered above, the mirror asymmetry of perovskite nanomaterials is imparted from small organic molecules with optical centers. Efficiency of chirality transfer and resulting properties including CPLE are strongly dependent on the mutual organization of MeX<sub>6</sub> octahedrons that is archetypally described as perovskite dimensionality (that is different from the dimensionality of the nanostructures). Three-dimensional (3D) perovskites refer to materials where the MeX<sub>6</sub> octahedra are packed into a cubic lattice producing compounds with general formula AMeX<sub>3</sub> with A being either an organic or inorganic cation located in the interstitial area located between four MeX<sub>6</sub> octahedrons. Two dimensional (2D) perovskites refer to the crystal lattices in which MeX<sub>6</sub> octahedra sharing a corner are arranged into sheets with organic cations separating them. One dimensional (1D) perovskites are based on MeX<sub>6</sub> octahedrons arranged into chains, while zerodimensional (0D) perovskite materials are composed of isolated MeX<sub>6</sub> octahedrons.<sup>[58]</sup> Mirror asymmetry can be imparted to all of them either by binding chiral organic ligands to the surface of perovskite NPs [61, 62] or by using chiral organic cations in the A sites. [60, 63, 64] Chiral organic ligands can be incorporated into the AMeX3 nanostructures during the synthesis by adding them to the reaction media<sup>[62, 65]</sup> or after their preparation by ligand exchange (Figure 2a).<sup>[62]</sup> Both methods have their advantages and their suitability for the synthesis of CPLE-active materials with strongest polarization rotation and PLQY is still being assessed. Their current values of |gcple| are comparable to those obtained for semiconductor NPs and metal nanoclusters. For example, the sonication of pre-made 10 nm NPs from CsPbBr<sub>3</sub> with R/S-2-aminooctane as surface ligands led to CPLE with  $|g_{CPLE}| = 1.1 \times 10^{-3}$ . [66] Lattices from octahedra may have numerous types of chiral distortions affecting both PLQY and geometry of molecular orbitals that can lead to non-linearity and non-additivity of seemingly obvious chirality transfer effects. For example, the NPs shown in Figure 2b displayed the maximum  $|g_{CPLE}| = 6.8 \times 10^{-2}$  when they carry *mixed* chiral and achiral ligands with optical asymmetry decreasing for NPs carrying only chiral or achiral ligands. [62]

The organic cations in 2D, 1D, and 0D perovskites can be bulky, while the interstitial cavities in 3D perovskites are too small to accommodate other cations except for Cs<sup>+</sup>, Rb<sup>+</sup>, MA<sup>+</sup>, and FA<sup>+</sup>. Hence, the chirality transfer from such organic ligands can be attained via surface modification of perovskites similarly to the chirality transfer observed for II-VI semiconductor<sup>[67]</sup> and ceramic NPs<sup>[68]</sup>. On the contrary, 1D, 2D, and quasi-2D perovskites have relatively open space to accommodate chiral amine cations into the inorganic framework. For 2D perovskites, the chiral amine cations intercalate between the sheets of interconnected MeX<sub>6</sub> tetrahedra, producing a material with alternating organic and inorganic layers. Inserted chiral molecules distort the crystal lattice of the perovskite. [51, 69, 70] 1D and 2D hybrid organic-inorganic perovskites most often acquire chirality through inducing chiral amine to the A site during synthesis. [62, 63, 71] In both cases, the incorporated chiral molecules lead to strong changes in quantum states responsible for optical effects with usually high CD peaks - in the range of 100 mdeg. However, chiroptical activity in absorption does not necessarily translate in high CPL and thus, CPLE for this type of nanomaterials, because the dot product between transition moments for electric and magnetic dipoles as well as probability of radiative and non-radiative transitions are difficult to predict without dedicated first principle calculations for all of them.

Hu et al. reported that perovskite R/S-MBAPbBr<sub>3</sub> bulk single crystals with sizes around 10 mm also show CD and CPLE peaks (**Figure 2c-e**). The obtained crystals are transparent and flat (**Figure 2c, 2e**). The CPLE activity could be classified as CPL-dominant because, in part, of the non-centrosymmetric geometry attributed to the interactions between the chiral MBA and Pb-Br-based non-centrosymmetric triangular pyramid.<sup>[72]</sup>. They belong to orthorhombic phases and with a space group  $P2_12_12_1$ .

Chirality can also be imparted to perovskite-based materials via ordered assembly of perovskite NPs onto chiral templates, which is also suitable for achiral and racemic mixtures of perovskite NPs. The assembly pathways are considered in *Section 3 (on CPS)*, and typically display strong CPLE activity.<sup>[73-75]</sup>

<u>CPL via non-linear optical effects:</u> Perovskites also afford combined linear and non-linear optical effects to increase the efficiency or tune the wavelengths of CPLE maxima. Upconverting NPs with a diameter of ~10 nm made from NaYF<sub>4</sub>: Yb were embedded into larger 20 nm NPs made from CsPbBr<sub>3</sub> capped with R/S-2-aminooctane(**Figure 2f-g**). [76] In this case, the host CsPbBr<sub>3</sub> perovskite NPs are acting as light absorbing 'chiral antennae' that adsorb the circularly polarized photons and transfer the excitation energy to the upconverting NP guests, leading to up-converted CPL. Thus, the excitation of 980 nm laser results in a CPL peak at 520 nm with  $|g_{CPLE}| = 4.5 \times 10^{-3}$ . [66]

Besides the incorporation of upconverting NPs, non-linear CPL can be based on the direct two-photon absorption (**Figure 2h-i**).<sup>[65]</sup> The excess bromide atoms in CsPbBr<sub>3</sub> NPs cause Br-rich defects, which bind amine ligands. These layers from chiral amines distort the packing of the atoms on the NP surface, leading to green CPL emission at 521 nm with the  $|g_{CPLE}| = 7.0 \times 10^{-3}$ . These NPs have a high two-photon absorption cross section at 800 nm up to  $3.68 \times 10^4$  GM, (1 GM =  $10^{-50}$  cm<sup>4</sup> s photon<sup>-1</sup>), which is two orders of magnitude higher than that for organic molecules.

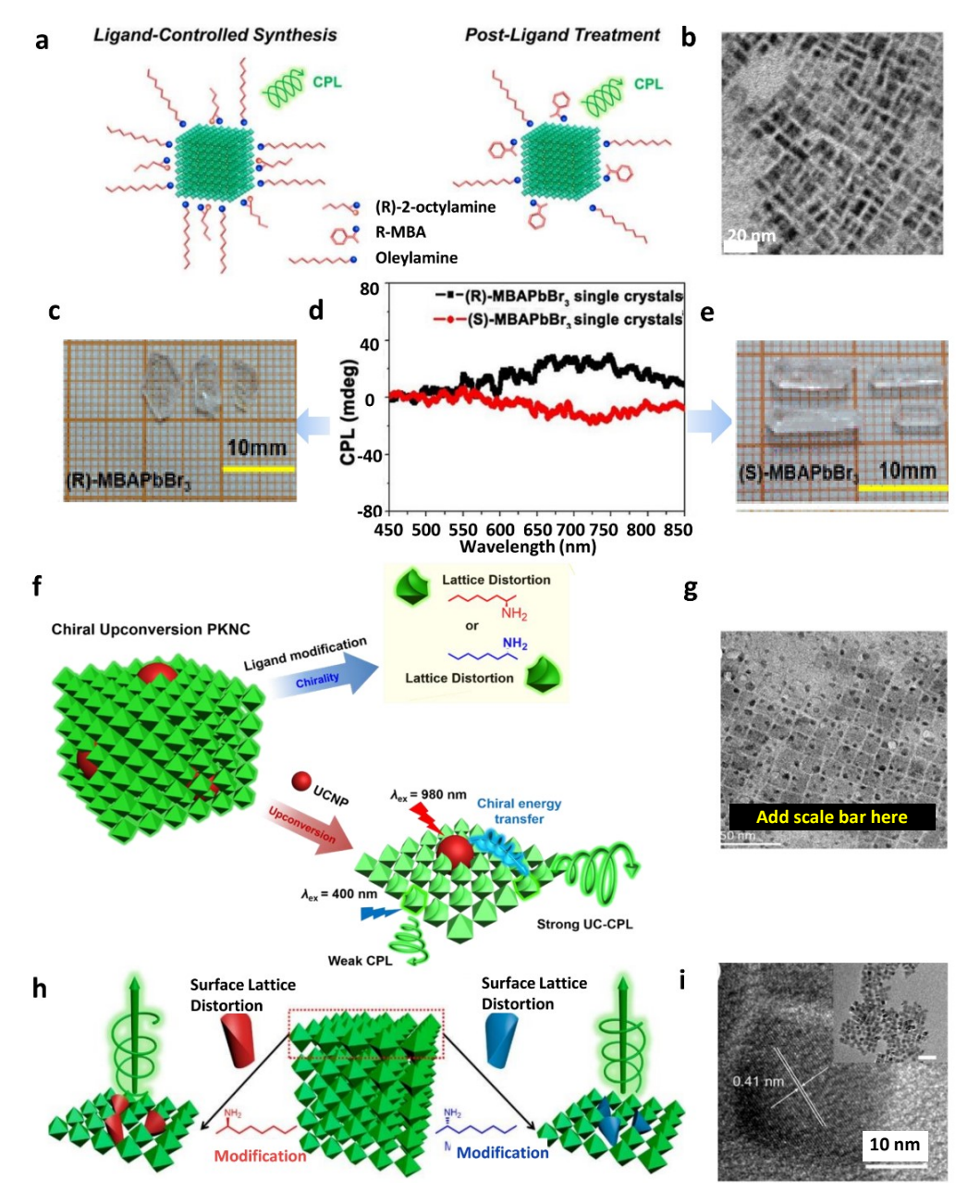


**Figure 2** CPL in perovskite nanostructures and single crystals. (a) Two synthetic methods to transfer chirality to perovskites: ligand-controlled synthesis and post-ligand treatment: (b) the corresponding TEM image of NPs with the highest CPL value. The CPLE-active macroscale chiral perovskite single crystals: photograph of *R*-MBAPbBr<sub>3</sub> (c) and *S*-MBAPbBr<sub>3</sub> (e) and the corresponding CPLE spectrum (d). (f) Illustration of chirality and

CPL in host-guest chiral composite with upconverting NPs: (g) the corresponding TEM images of host perovskite NPs incorporating upconverting NPs. The energy transfer between upconverting NPs and perovskite NPs in the chiral composite amplified the green CPL with a four-fold magnification of |*g*<sub>CPLE</sub>| value excited by 980 nm laser. (h) Schematic illustration of the origin of chirality in chiral CsPbBr<sub>3</sub> perovskite NPs with two-photon upconverted circularly polarized luminescence. (i) HRTEM image of perovskite NPs with right-handed emission. The insert shows the corresponding TEM image and the scale bar is 100 nm. (a)-(b) Reproduced with permission. [62] Copyright 2020, American Chemical Society. (c)-(e) Reproduced with permission. [72] Copyright 2020, American Chemical Society. (f)-(g) Reproduced with permission. [66] Copyright 2021, Springer Nature. (h)-(i) Reproduced with permission. [65] Copyright 2019, American Chemical Society.

Almost all previously reported perovskites were synthesized in an organic phase, which limits the choice of available ligands, makes perovskite nanostructures more expensive, and is problematic for environmentally conscious technologies. To solve the problem, aqueous preparation methods were developed. Li et al. prepared 2D (MBA)<sub>2</sub>PbI<sub>4</sub> and 1D (C<sub>4</sub>N<sub>2</sub>H<sub>14</sub>PbI<sub>4</sub>) perovskites in water (**Figure 3a-b**).<sup>[63, 64]</sup> The films of these perovskites were made by spin-coating on quartz slides for the absorption, polarization, and emission measurements. An optical technique different than the traditional CPL spectroscopy (Section 1.2) was applied to characterize these materials. Here, the samples were excited by a linearly polarized laser light and their PL displayed strong circular polarization for (R-MBA)<sub>2</sub>PbI<sub>4</sub> and (S-MBA)<sub>2</sub>PbI<sub>4</sub> (**Figure 3c**), while no difference in left-handed ( $\sigma$ <sup>-</sup>) and right-handed ( $\sigma$ <sup>+</sup>) circularly polarized light emission intensity was observed for (rac-MBA)<sub>2</sub>PbI<sub>4</sub>. Note that this is a different measurement technique than CPL and the optical asymmetry here is reported in terms of degree of circular polarization, DP, defined in Eq. (2)

$$DP = \frac{I_{\sigma^{-}} - I_{\sigma^{+}}}{I_{\sigma^{-}} + I_{\sigma^{+}}} 100\%$$
 (2)

where  $I(\sigma^-)$  and  $I(\sigma^+)$  are the intensity of the emitted  $\sigma^-$  and  $\sigma^+$  PL, respectively. The films from C<sub>4</sub>N<sub>2</sub>H<sub>14</sub>PbI<sub>4</sub> 1D perovskites showed an average DP = 3.8% at 77 K. The optical asymmetry is associated for these films with distorted lattice due to stacking of two-dimensional hydrogen-bonded layers biased by tunable halogen bonds. [64, 77]

The molecules of the chiral amine were incorporated into the crystal structure of 2D perovskites with a general formula  $(R-/S-MBA/PEA)_2PbI_4$  where  $C_6H_5C_2H_4NH_3$  imparted chirality to the packing of  $[PbI_6]^4$ -layers (**Figure 3d-e**). The film coated on the quartz slides showed strong CD amplitudes around 100 mdeg<sup>[63]</sup> and were CPLE-active especially at low temperatures, which is indicative of CPL-dominant CPLE process. The enantiomers showed a DP = 10% at 77 K with the maximum value of 17.6% for  $(S-MBA)_2PbI_4$  (**Figure 3f-g**). The intensity of CPL increased significantly with decreasing temperature due to temperature-dependent spin reversal.<sup>[63]</sup>

Lin et al. recently reported that the chiral 2D hybrid organic-inorganic perovskites synthesized by halogenation of the organic ions in the A site.<sup>[78]</sup> They used a halogen-substituted (with F, Cl, Br and I atom) phenyl group at the para-position to prepare the 2D perovskites and results show that most of them could be both CD- and CPL-active at room temperature. Among them, the perovskite having a Cl-substituted chiral cation exhibits the highest CD and CPL intensities whereas the F-substituted ones show the weakest intensities. The reason could be the varied magnetic transition dipole of 2D perovskites, which is sensitive to the *d*-spacing between inorganic layers and the halogen–halogen interaction between organic cations and the inorganic sheets.<sup>[78]</sup>

Nuzzo and co-workers employed the chiral derivate of 1-(1-naphthyl)ethylamine, S/R-NEA, as the chiral A site to synthesize reduced dimensional Ruddlesden-Popper perovskite films, which showed CPLE activity at room temperature, with the  $|g_{CPLE}| \sim 3 \times 10^{-3}$  attributed to the recombination of excitons (**Figure 3h-i**).<sup>[79]</sup> Their experiment proved that S/R-NEA impart chirality to the electronic structure of perovskites causing optical asymmetry in the emitted photon.

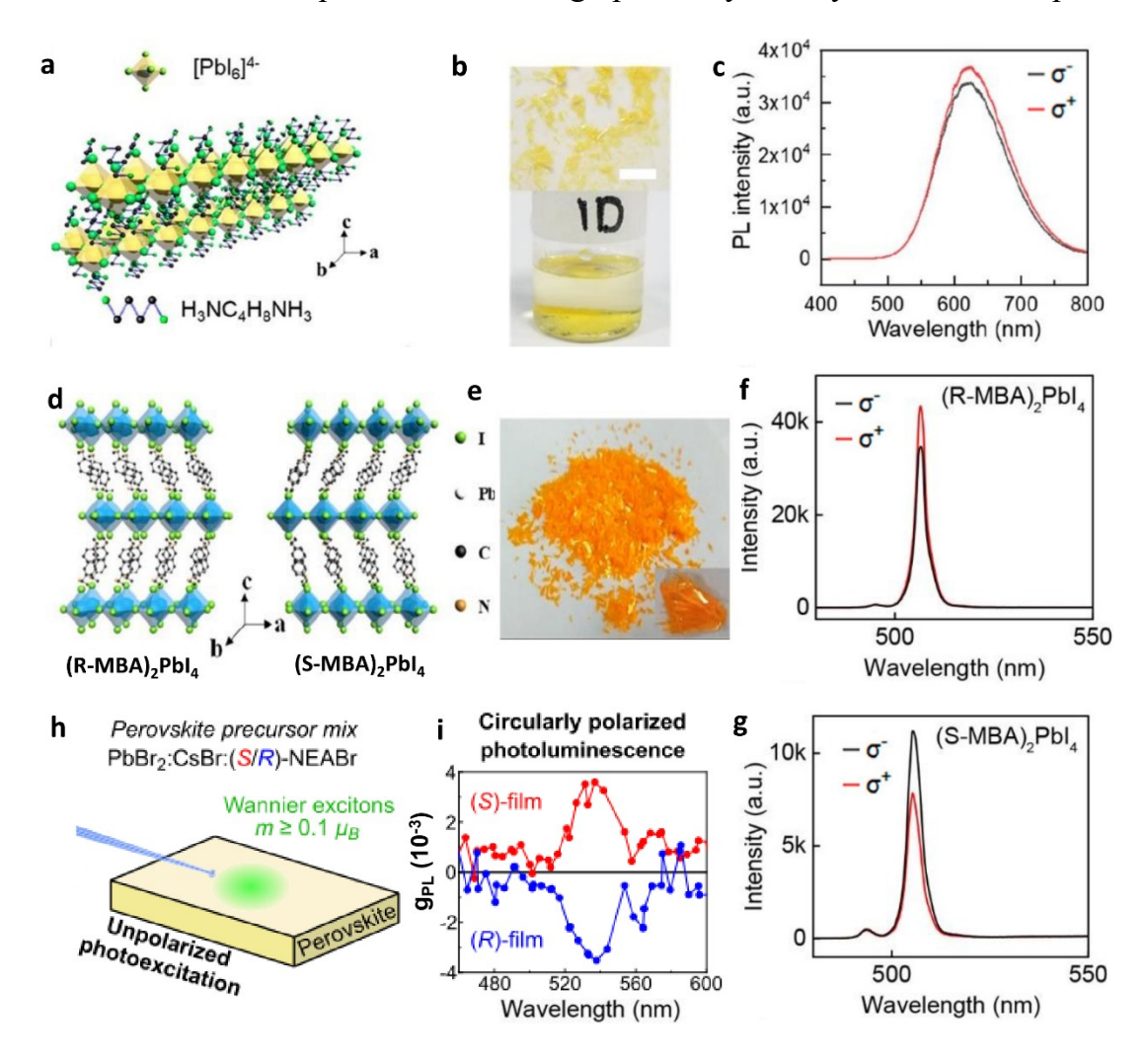


Figure 3 CPL-dominant CPLE for chiral 1D and 2D perovskites. The crystal structure (a) and image (b) and CPL emission at 77 K (c) of 1D perovskite C<sub>4</sub>N<sub>2</sub>H<sub>14</sub>PbI<sub>4</sub>. The crystal structures (d) and image (e) of (R-MBA)<sub>2</sub>PbI<sub>4</sub> The polarization-sensitive PL spectra of (R-MBA)<sub>2</sub>PbI<sub>4</sub> (f) and (S-MBA)<sub>2</sub>PbI<sub>4</sub> (g). Schematics of optical excitation in Ruddlesden–Popper perovskite films (h) and (i) |*g*<sub>CPLE</sub>| spectrum. (a)-(c) Reproduced with permission. <sup>[64]</sup> Copyright 2019, American Chemical Society. (d)-(g) Reproduced with permission. <sup>[63]</sup> Copyright 2019, American Chemical Society. (h)-(i) Reproduced with permission. <sup>[79]</sup> Copyright 2020, American Chemical Society.

<u>Toxic-metal-free perovskites.</u> Most reported CPL-active perovskites contain toxic Pb atoms in the Me sites, which is undesirable. Fu et al. reported the lead-free S/R-3-(fluoropyrrolidinium)MnBr<sub>3</sub> with  $|g_{CPLE}| = 6.1 \times 10^{-3}$  in the range 550 to 725 nm. Another interesting aspect of these materials is that S/R-3-(fluoropyrrolidinium)MnBr<sub>3</sub> represents the first case of chiral perovskite ferroelectrics.<sup>[80]</sup> The transition between paraelectric and ferroelectric phases occurs at 273 K and both of them are enantiomorphic exhibiting the same  $g_{CPLE}$  of the same modulus but of opposite signs.

Beard et al. replaced Pb with Sn in the Me sites to synthesize (*R/S*-MBA)<sub>2</sub>SnI<sub>4</sub> 2D perovskite films with a thickness of 50-60 nm. Although they focused on spin-polarization yet this material was CPLE-silent.<sup>[81]</sup> These and similar studies give a pathway to lead-free perovskites with CPLE property.<sup>[82]</sup> There are other reports about chiral perovskites, which all show high CD and promising chiral induced spin and so on, even though they lack the research of CPLE.

### 3. Nanomaterials with Scattering-Dominant Circularly Polarized Light Emission

## 3.1. Assemblies of chiral nanoclusters

Some nanostructures are CPLE-silent but have strong PL. In order to gain polarization rotation of the emitted photons, one can take advantage of CPS. The individual nanostructures can be assembled which results in CPS-dominant CPLE. For example, individual Au nanoclusters, capped with chiral ligand (R)- or (S)-2,2'-bis(di-p-tolylphosphino)-1,1'-binaphthyl, (R)- or (S)-Tol-BINAP, display CD spectra but no CPLE activity.<sup>[33]</sup> However, when they self-assembled into uniform body-centered nanocubes with an average size of 100 nanometers (**Figure 4a**), the non-luminescent Au clusters progressively became highly luminescent with emission peaking at 583 nm (**Figure 4b**). The clusters also showed CPLE activity with the highest  $|g_{CPLE}|$  value of  $7 \times 10^{-3}$  (**Figure 4c**). The microsecond PL decay time and the large Stokes shift of approximately 138 nm clearly suggest that the PL of clusters originates from the long-living excited states that are likely to be either

ligand-to-metal charge transfer (<sup>3</sup>LMCT) or a ligand-to-metal-metal charge transfer (<sup>3</sup>LMMCT) triplets.

A similar case of the transition from CPLE-silent to CPLE-active states upon assembly can be found for AuAg bimetallic nanoclusters. [34] The adenosine 5'-monophosphate capped AuAg nanoclusters show PL at 475 nm but are CPL-silent. When they self-assemble into a helical structure in the presence of a guanosine 5'-monophosphate chiral template, they show CPLE activity and the  $|g_{CPLE}|$  co-assembly has a width of 200 nm and a length of several micrometers, leading to strong scattering of light, which indicates that the CPLE activity comes from CPS and could be regulated with  $K^+$  ion, obtaining the maximum value up to  $2.7 \times 10^{-2}$ . In addition to noble metals, the layered assemblies of organic-inorganic hybrid R-/S-phosphine-copper iodide hybrid nanoclusters also exhibit CPLE activity in crystalline states. [83] The nanoclusters assembled into two kinds of assemblies under the intermolecular interactions were formed, hexagon platelet-like microcrystals ( $|g_{CPLE}| \approx 9.5 \times 10^{-3}$ ) and highly oriented crystalline film ( $|g_{CPLE}| \approx 5 \times 10^{-3}$ ). An electroluminescent device was successfully prepared with the CPLE-active thin film, obtaining a satisfactory luminance of 1200 cd m<sup>-2</sup>. [83]

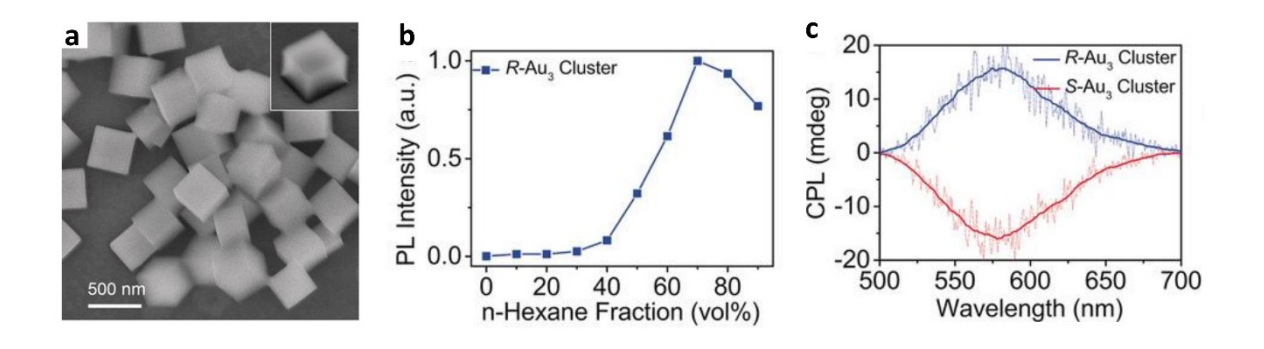


**Figure 4.** CPLE of nanoassemblies from chiral Au nanoclusters. (a) (SEM) image of cubic assemblies of Au<sub>3</sub>[(R)-Tol-BINAP]<sub>3</sub>Cl cluster in dichloromethane with 70% *n*-hexane. (b) PL spectra of Au<sub>3</sub>[(R)-Tol-BINAP]<sub>3</sub>Cl clusters in dichloromethane with various *n*-hexane contents. (c) CPLE spectra of Au<sub>3</sub>[(R)-Tol-BINAP]<sub>3</sub>Cl (blue curve) and Au<sub>3</sub>[(S)-Tol-BINAP]<sub>3</sub>Cl (red curve) nanoassemblies in 70% *n*-hexane. (a-c) Reproduced with permission. [33] Copyright 2017, Wiley-VCH.

#### 3.2. Light-emitting superstructures with multiscale chirality

Chiral nanostructure based on twisted gold cysteinate nanosheets showed strong CPLE in the visible and near-IR parts of the spectrum with the maximum  $|g_{CPLE}| = 0.01$  at 620 nm (**Figure 5**). The mechanism of the CPLE in this system was thoroughly evaluated based on experimental and modelling data. The circular polarization of the emitted photons from these complex hierarchically organized particles has contributions from both CPL and CPS. The basic structural unit of these particles are gold cysteinate nanosheets. Due to the strong Au-Au interactions in the gold sulfide monolayers serving as a 2S skeleton of these nanosheets, they have strong PL at 620 nm. The chirality of organic molecules covalently bonded to them is transferred to the quantum states of these nanosheets leading to the emission of circularly polarized photons (**Figure 5c** and **5d**). Importantly, the spiky geometry of these particles enables them to be reversibly dispersed in a variety of solvents from very hydrophilic (methanol) to very hydrophobic (toluene) (**Figure 5g**). The red PL from these chiral nanosheets is also pH-resilient and can be observed from very basic to very acidic media (**Fig. 5h**).

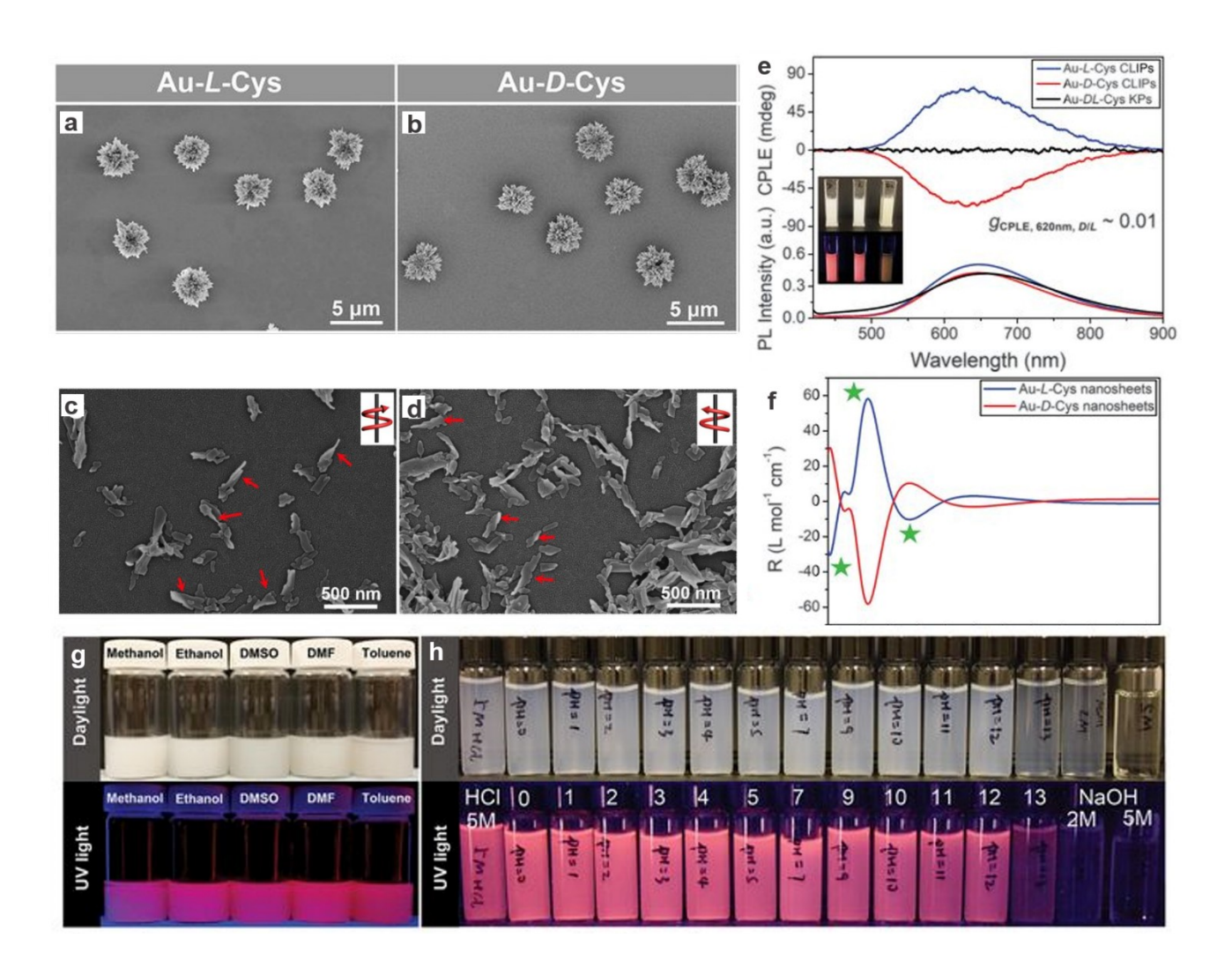


**Figure 5** CPS-dominant CPLE for light-emitting superstructures from Au-S with nanosheets with multiscale chirality. SEM images of Au–*L*-Cys (a) and Au–*D*-Cys (b) chiral hedgehog particles and corresponding CPLE spectra (e). SEM images of Au–*L*-Cys (c) and Au–*D*-Cys (d) hedgehog particles after 15 min of sonication that result in individual twisted ribbons forming spikes in complete chiral hedgehog particles. The computational differential extinction spectrum (f) for the differential scattering contribution to the chiroptical properties of the CLIPs at long wavelengths. (g) Dispersions of Au–L-Cys CLIPs in different solvents [methanol, ethanol, dimethyl sulfoxide (DMSO), *N*,*N*-dimethylformamide (DMF), and toluene]. (h) Stability study of Au–*L*-Cys dispersions with different pH values or concentrations of HCl or NaOH after 12 hours. (a-h) Reproduced with permission. [17] Copyright 2020, AAAS.

When the surface ligands are changed from *L*-cysteine to *D*-cysteine, the direction of the polarization is also changed. Doping these Au-S nanosheets with Ag and Cu can also tune the wavelength of the emission while retaining the sign of the circular polarization. The PL peaks shifted from red (620 nm) to orange (580 nm) and yellowish-green (550 nm) upon Cu and Ag doping (Cu/Au = 3.3% and Ag/Au = 16.5%), respectively, with the wavelength change of CPLE spectra. CPL from the optical centre on the nanosheets is subsequently scattered on the dispersed particles with submicron chirality and this process can strongly alter the degree and the sign of the circular polarization. In the case of the fully assembled chiral hedgehog particles, the contribution from CPS increases considerably compared to the individual nanosheets. The additional contribution from CPS actually changes their polarization rotation to the opposite. The change of the helicity of the nanospikes in the chiral hedgehog particles reverses the sign of the circular polarization of the CPLE from their dispersions.<sup>[17]</sup>

Hierarchical structures combining photoluminescence centers and microscale scatterers can also be grown on solid substrates. Che and coworkers<sup>[84]</sup> reported amino acid-induced growth of chiral ZnO films of micron scale on quartz slides. The chiroptical activity comes from the three levels of hierarchical assemblies: 1) coiled nanoplates of ZnO crystals with a length of 0.5-1.5 μm and thickness of about 20 nm; 2) helical stacking of the nanoplates with a pitch of about 30 μm; and 3) flower-like nanostructures. Similarly to chiral hedgehogs, the natural PL of ZnO can be combined here with CPS from chiral superstructures that also generate high CD values beyond the limit of detection of CD spectroscopy within 300-379 nm and is over 1000 mdeg around 400 nm. The maximum CPL intensity was observed at -470 mdeg. The authors did not report tuning of the CPLE although it should be possible.

## 3.3 Nanoassemblies on Templates

As can be seen from the example of assemblies of nanoclusters and superstructures considered above, CPS-dominant CPLE typically occurs when the chiral nanostructures acquire chirality in the scale comparable with the incident light wavelength. Chirality at nanometer and longer scales is attained by the assembly of nanocarbons into chiral superstructures<sup>[85]</sup> exemplified by the assembly of nitrogen-doped carbon dots (NCDs) on chiral gels based on L/D-glutamic<sup>[36]</sup> that produces helicoids with a typical pitch length around 0.5  $\mu$ m. The NCDs attach through noncovalent bonds onto the chiral gel template forming chiral microscale assemblies with CPLE activity originating from CPS of photons emitted by the luminescent NPs (**Figure 6a-b**). Varying the excitation wavelength from 350 nm to 370 nm, the CPLE intensity of such composite gels is adjustable due to the characteristic optical properties of nanocarbons<sup>[86]</sup> with the  $|g_{CPLE}|$  varying from  $2 \times 10^{-3}$  to  $4 \times 10^{-3}$  (**Figure 6c**).

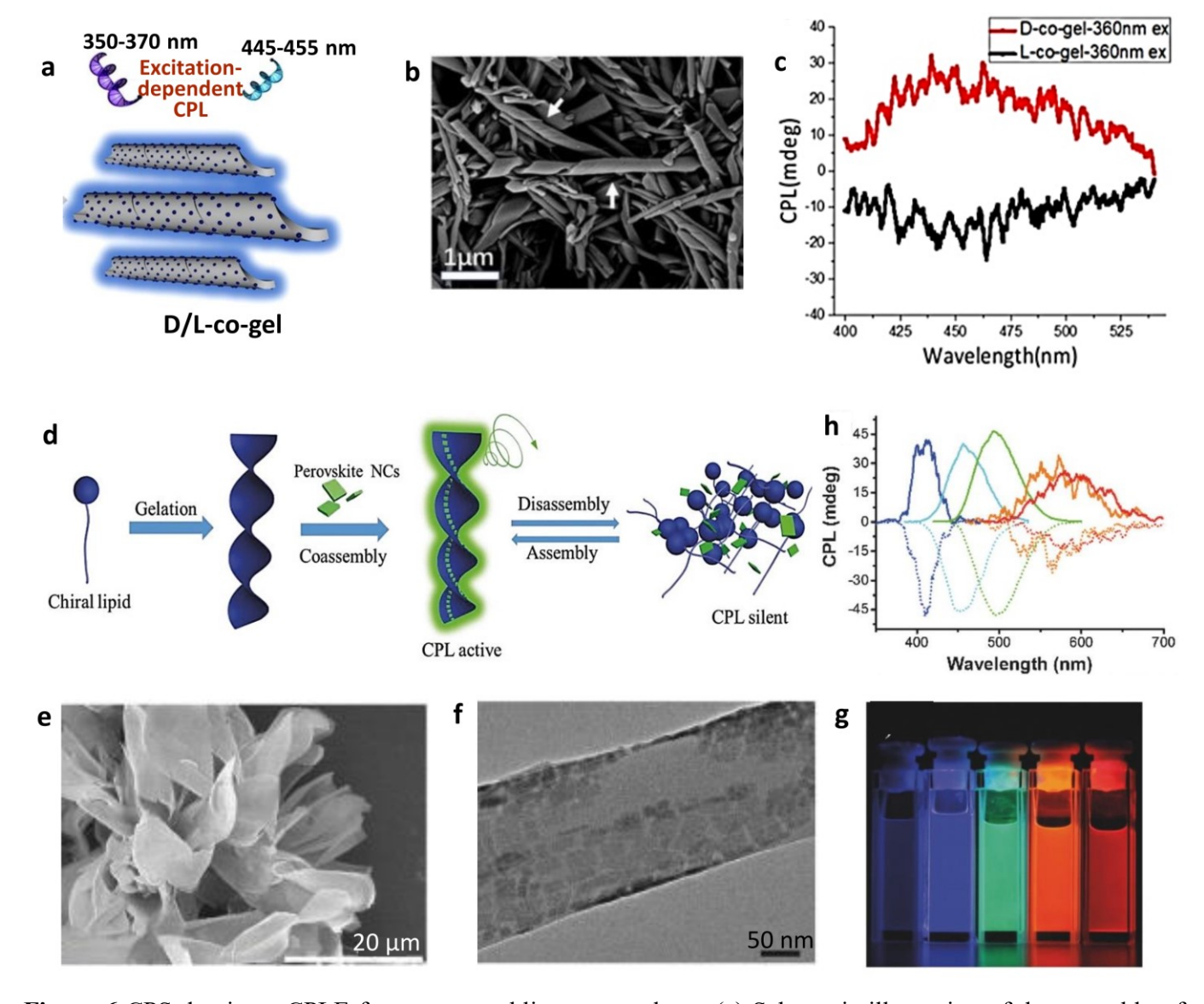


**Figure 6** CPS-dominant CPLE for nanoassemblies on templates. (a) Schematic illustration of the assembly of carbon dots onto the surface of the chiral gelator template with CPS. (b) FE-SEM image of D-co-gel (typical helices and tubular terminal are highlighted by arrows) (c) CPLE spectrum of L-/D-co-gel under 360 nm. (d) Illustration of the assembly process of perovskite and chiral gels. (e) SEM image and (f) TEM image of DGAm/CsPbBr<sub>3</sub> NPs. (g) Photograph of colloidal dispersions of CsPbX<sub>3</sub> NPs with different halides (X = Cl, Br, and I) in hexane under UV light. (h) The mirror-image CPL spectra of co-assembly samples of CsPbX<sub>3</sub> NPs doped chiral gels with different halide ions (X = Cl, Br, and I). The solid lines and dash lines correspond to a pair of symmetric chiral assembly samples. (a-c) Reproduced with permission. [36] Copyright 2020, American Chemical Society. (d-h) Reproduced with permission. [73] Copyright 2018, Wiley-VCH.

The same mechanism can be realized for other nanoscale emitters, for instance, nanoscale perovskites. A pair of chiral lipids, *N*, *N*'-bis(octadecyl)-*L*/*R*-glutamic diamide were used as the gelators.<sup>[73]</sup> The achiral perovskite NPs with the size of 10-15 nm and chiral gelators assemble into chiral gels with undetermined helical geometries in micron scale (**Figure 6d-f**). Changing the

halogen (Cl, Br, I) in the X site, the CPLE colors can be varied (**Figure 6g-h**), which can be used to engineer CPLE-active materials with a broad range of circular polarization.<sup>[73]</sup> Achiral upconverting NPs can also be assembled into CPLE-active composites in a similar fashion. Their co-gelation with spiral nanotubes results in intense CPLE from the UV to NIR region, which is advantageous for new chiral optical devices.<sup>[87]</sup>

## 3.4 Chiral Nanocomposites

As we mentioned above, achieving simultaneously high optical asymmetry and intensity of CPLE is one of the goals of this research filed of chiral photonics. Chiral nanocomposites made from two or more materials with hierarchical organization similar to the chiral hedgehogs shown in **Figure 5** but manufactured in a top-down process open possibilities to combine PL emitters with CPS-active nanoscale and microscale structures. This approach provides a convenient, generic, and simple pathway to engineer new CPLE-active materials.

Mesoscale and microscale helicity can also be imparted in a top-down assembly process, which is convenient for manufacturing nanocomposites. PL-active achiral CdTe nanowires with a diameter of about 8 nm and a length of about 500 nm, prepared using the methods described by Z. Tang et al., [88] were incorporated into composite fibers from CaCO3 or graphene twisted during the extrusion process.<sup>[89]</sup> Each fiber is made from platelets with a lateral size of 4-45 µm and thickness of 1-500 nm producing hierarchical Bouligand composites with pitches about 150 μm and 20 μm in the axial and transversal direction of the fibers, respectively. Achiral CdTe nanowires incorporated in the matrix of the nacre-like fibers with hierarchical twists acquire the circular polarization from the CPS on the Bouligand substructure of the fibers. The sign of the polarization rotation is determined by the left or right rotational sense of the fiber. The left-handed and righthanded helical fibers can be produced by controlling the spinning direction and thereby the emitted L-CPLE or R-CPLE (Figure 7a-b). Since the helicity of the fibers is dependent on its deformation, externally applied strain enables one to vary the polarization rotation. CPLE arising from helical patterns of the multiscale deformations can be controlled by applying different tension to the fibers, which can be used for the remote read-out of the strain. As the fiber is stretched from its original length to 1.5 and 2 times of its original length, the  $|g_{CPLE}|$  value decreases from  $3.7 \times 10^{-3}$  to  $2.8 \times 10^{-3}$  $10^{-3}$  and finally to  $1.3 \times 10^{-3}$  (Figure 7c-d). [89]

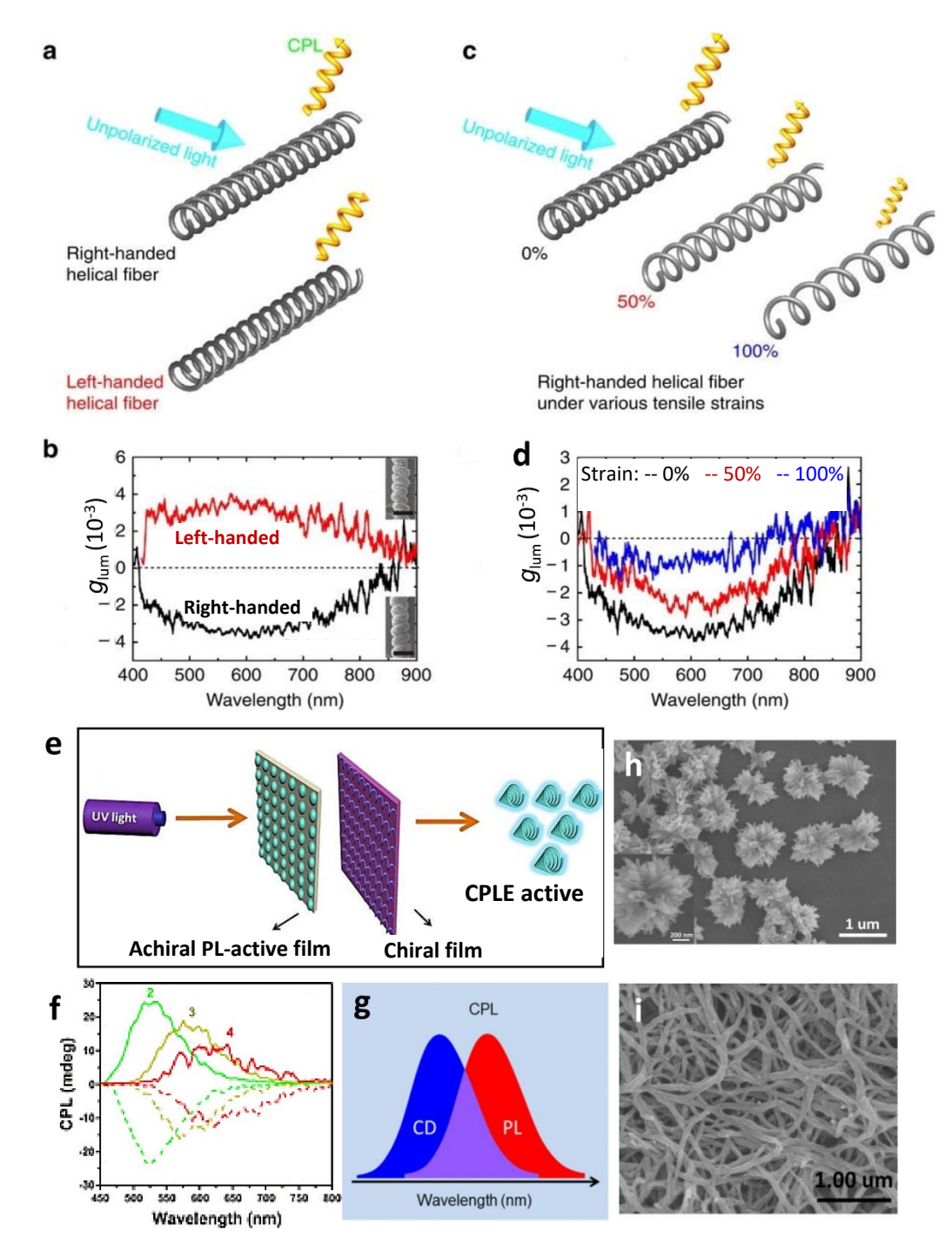


**Figure 7** SPS-dominant CPLE for chiral nanocomposites. Illustration of right-handed and left-handed PVA/CaCO<sub>3</sub>/CdTe helical fiber due to opposite spinning directions (a) and corresponding CPLE spectra (b). Illustration of fibers at different tensile strains of 0, 50 and 100% (c) and corresponding CPLE spectra (d). (e) Illustration of the relative position between fluorescent component and chiral component to obtain CPLE. (f) Mirror-image CPL spectra of three kinds of fluorescent achiral and chiral films excited at 320 nm. (g) Schematics of the spectral overlap for the CD and PL spectra is necessary for intense CPLE. (h) SEM image of CuO+cellulose nanoassemblies with complex corrugated geometries ("nanoflowers"). (i) SEM images of chiral polymer

nanofibers. (a-d) Reproduced with permission. [89] Copyright 2016, Springer Nature. (e-i) Reproduced with permission. [18] Copyright 2020, American Chemical Society.

Similar light-matter interactions based on CPS are the foundation of polymer/perovskite composite nanofibers made by electrospinning. Here, helical polyacetylene nanofibers with a diameter of 180 nm and a length in micron scale serve as chiral scatterers while perovskite NPs are likely to serve as emitters. The nanofibers produce CPLE-active composites with  $|g_{CPLE}| = 3.2 \times 10^{-2}$  [90]

Deng et al. combined chiral components and achiral fluorescent materials obtaining CPLE with  $|g_{CPLE}| = 0.323$  (Figure 7f). [18] The chiral components could be organic polymer nanofibers, CuO nanoflowers, organic-inorganic composites from CuO and cellulose (Figure 7h-i). One of the key indicators that CPLE here is dominated by CPS is that the sequence of the light-matter interactions and thus the media on the path of the light beam is key to achieving CPLE activity. If the incident light passes through PL material first and then the chiral material, the CPLE could be generated but not if the opposite order is used (Figure 7e). The wavelength overlap of PL spectra of the emitter and the CD spectra of the chiral component is the necessary factor to generate CPLE. The intense bisignate peak at 400 nm arises from the CPS of the nanofibers. To prove this, films with varied chiral polymer concentrations were prepared. As expected, the higher the concentration of nanofibers results in higher CD intensity because CPS from Mie scattering increases with the increasing concentration of nanofibers. To elucidate the generation of CPLE, several possible sources have been excluded, including chiral transfer, selective absorption of light by chiral component, circularly polarized reflection, leaving CPS as the dominant contribution to CPLE. CPLE with variable spectral maximum was obtained by changing PL and chiral materials.<sup>[18]</sup> CPLE composites also allowed optimization of the overlap between PL spectra of the PL component and CD spectra of the chiral component, which is very convenient for device fabrication (Figure 7g). [91]

### 3.5 Chiral composites with photonic bandgap

Photonic crystals represent a rapidly developing versatile platform for engineering CPLE-active materials with dominant CPS contribution. Most common among these are the cellulose-based nanocomposites that self-assemble into chiral liquid crystalline (LC) phases<sup>[16]</sup> that incorporate PL-active components. These kinds of materials typically have high  $|g_{CPLE}|$  values because transmission of photons with one helicity is forbidden due to polarization-dependent photonic bandgap in some LC phases.<sup>[14-16]</sup> For cellulose, the  $g_{CPLE}$  values are negative, because the transmission of left-

handed photons is forbidden while right-handed photons are allowed to pass. Several kinds of fluorescent materials, including carbon dots, semiconductor NPs, noble metal NPs, silica, upconverting NPs, and perovskites, have been incorporated into the cholesteric structure and investigated for CPLE.<sup>[14, 15, 74, 92-98]</sup>

In this category of CPLE-active materials, the organization of carbon dots with cellulose forming the cholesteric LC in the nature-inspired nanocomposites is particularly popular. [14, 15, 74, 92-98] Among them, Xu and co-workers showed strong right-handed CPLE with  $|g_{CPLE}|$  up to  $7.4 \times 10^{-1}$ <sup>1</sup>.[94] The multicolor tunability of CPLE was achieved through changing carbon dots and photonic bandgap. Tsukruk and co-workers showed a  $|g_{CPLE}|$  value of  $2.0 \times 10^{-1}$ . They fabricated the freestanding chiral fluorescent patterns via inkjet printing of the chiral hybrids. [96] Liu et al. reported the  $|g_{CPLE}|$  value of 2.7  $\times$  10<sup>-1</sup>. [14] Besides, it showed circular polarized room-temperature phosphorescence with a long lifetime of 103 ms and corresponding dissymmetric factors to -0.47.<sup>[14]</sup> When the achiral A high value (1.6) of  $|g_{CPLE}|$  was achieved when the achiral perovskites were assembled into cholesteric superstructure stacks (Figure 8a). The overall assembly achieved a very high circular polarization conversion efficiency, leading to impressively high |gCPLE| values. The CPLE could be controlled easily with the regulation of angle. [74] Silica also could assemble with cellulose NPs to form chiral nematic films after the removal of cellulose, which has a |gCPLE| value of 3.8× 10<sup>-1</sup> and multi-color and on-off switchable CPLE activity.<sup>[15]</sup> The UC-CPLE has been achieved after the integration of upconverting NP into cellulose NP-based chiral photonic films. The photonic with the addition of glycerol. Moreover, the film showed humidity responsive  $|g_{CPLE}|$ value.[97]

CdSe/CdS and ZnS/CdSe NPs have also been assembled into the cellulose NP films (**Figure 8b**). [92, 93] The photonic band gaps could be controlled by the glycerol content, which consequently regulated the  $|g_{CPLE}|$  values from  $2.1 \times 10^{-1}$  to  $4.8 \times 10^{-1}$ . The photonic nanocomposite films can be technologically attractive as optical labels to encode and decode information. The right-hand circularly polarized light can pass through the photonic film but the left-hand circularly polarized light cannot. Therefore, the code could be seen through the right-handed circularly polarized filter compared with the left one. (**Figure 8c**). [92] Duan et al. found that the addition of achiral perovskite NPs and achiral upconverting NPs into chiral liquid crystal enhanced CPLE resulting from the energy transfer from upconverting NPs to perovskite. [75] A  $|g_{CPLE}|$  as high as 1.1 is achieved when the perovskite's emission peak is at the center of the chiral liquid crystal's photonic bandgap. Moreover, the up-converted CPLE and radiative energy transfer could be regulated by the outside electric field.

The incorporation of PL-active guests into chiral nematic photonic crystals from cellulose often gives unusually high values of  $|g_{CPLE}|$ . These materials were engineered to maximize the degree of photonic bandgap overlap with PL wavelength. If there is no overlap, there is no CPLE activity. [92] The emission intensity and wavelength could be regulated through the PL wavelength of doped NPs or silica. [15, 92, 93] The thickness of film affects  $|g_{CPLE}|$  values: the  $|g_{CPLE}|$  rises because the transmission of the left-handed circularly polarized light is partially forbidden and its total becoming smaller with increased thickness, leaving relative pure right-handed circularly polarized light after the passing the chiral media. [15, 92] Similarly, Gao et al. reported the metal-enhanced CPLE of self-assembled Au@SiO2 triangular nanoprisms and fluorophores in chiral cellulose films. By overlapping the plasmon bands of Au@SiO2 triangular nanoprisms and the excitation–emission spectra of fluorophores, both the fluorescence intensity and  $|g_{CPLE}|$ value are significantly enhanced. The addition of sulforhodamine 101 and methylene blue leads to nearly fourfold and twofold increase of |gcple|, respectively, which brings new inspiration for the generation of superior CPLE. [98] Wang et al. reported the self-assembly of Ag nanorods coated with a continuous layer of SiO<sub>2</sub>, and a layer of 10 nm CsPbBr<sub>3</sub> NPs distributed over the nanorods (**Figure 8d**). The coated nanorods had diameters of 80 nm and lengths of 10 nm and displayed curved geometry that led to the formation of islands of chiral nematic liquid crystalline phases. The authors also prepared these nanorods with and without a layer of L- or D-cysteine deposited between SiO<sub>2</sub> and CsPbBr<sub>3</sub> (Figure 8d-e). [99] Considering the same sign of the 420 nm peak in CD spectra for L- and D-Cys, one can firmly conclude that the chiroptical activity at this wavelength originates from the meso- and microscale organization of the LC phase of the bent nanorods rather than the chirality of the cysteine coating. The CD peaks in 200-300 nm range display opposite signs for L- or D-cysteine indicating the optical activity of the chiral carbon centers in the surface ligands that fail to transfer the chirality to the perovskite or the LC phase of the nanorods (**Figure 8f**). These findings also show a greater role of light-matter interactions related to scattering rather than to emission from the quantum confined states for such systems. While PL intensity of 10 nm CsPbBr<sub>3</sub> NPs was enhanced by 87-fold because of the local surface plasmon resonance field enhancement effect of Ag nanorods. We note that the potential translation of these nanomaterials to LED devices is possible, even though the authors did not report CPLE.[99]

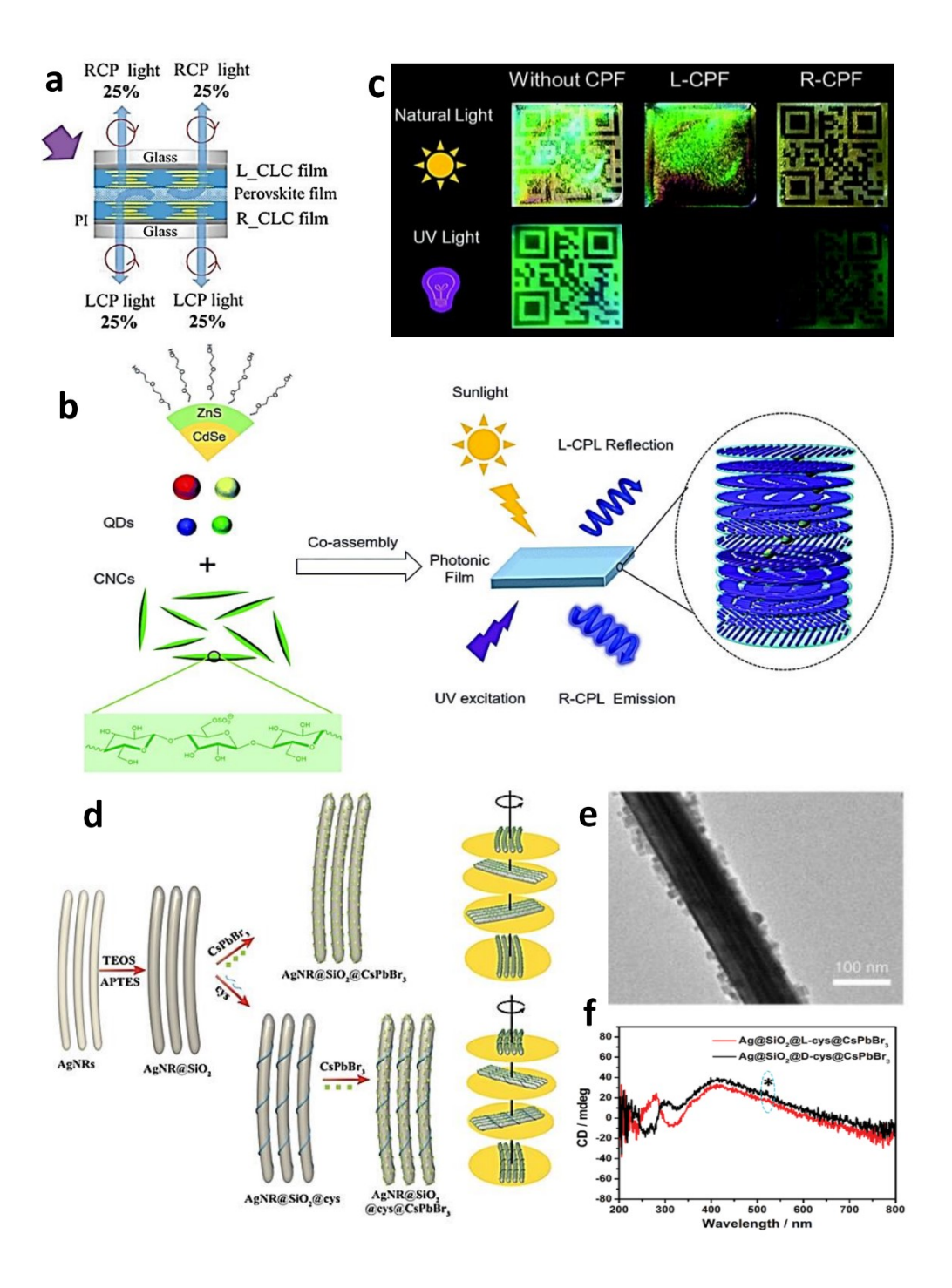


Figure 8 Chiral composites with photonic bandgap. (a) Cholesteric stack from CsPbX<sub>3</sub> perovskite nanoplatelets . The unpolarized light emission from the system converts to fully chiral light luminescence using this structure. (b) Illustration of CPLE-active photonic films obtained by the co-assembly of cellulose nanofibers and semiconductor NPs. (c) Photographs of CPLE-active photonic films placed under natural light on a quick response code. The images are taken using a nanocomposite without a circular-polarization activity (left), and with left-handed rotation (middle) and a right-handed rotation (right) (top) and UV light (down) respectively. CPF refers to circularly polarized filter. (d) The schematic illustration of the synthesis of Ag nanorods coated with SiO<sub>2</sub> and

CsPbBr<sub>3</sub> and those with an additional layer of *L*-cysteine between SiO<sub>2</sub> and CsPbBr<sub>3</sub> denoted as Ag@SiO<sub>2</sub>@cys@CsPbBr<sub>3</sub>. (e) TEM image of Ag@SiO<sub>2</sub>@*L*-cys@CsPbBr<sub>3</sub>. (f) The CD spectra of Ag@SiO<sub>2</sub>@*L*-cys@CsPbBr<sub>3</sub> and Ag@SiO<sub>2</sub>@*D*-cys@CsPbBr<sub>3</sub>. The star denotes the spectral position of excitonic transition in CsPbBr<sub>3</sub>. (a) Reproduced with permission<sup>[74]</sup> Copyright 2019, Wiley-VCH. (b)-(c) Reproduced with permission.<sup>[92]</sup> Copyright 2019, The Royal Society of Chemistry. (d)-(f) Reproduced with permission.<sup>[99]</sup> Copyright 2020, Wiley-VCH. Image notations are verbatim reproduction from the original publications.

#### 4. Conclusions and Outlook.

CPLE-active nanostructures have experienced rapid growth in research interest due to their promising future in information storage, imaging, biosensing, 3D displays, and other fields. Here we survey the progress achieved in CPLE photonics considering CPL and CPS mechanisms, which involve light-matter interactions at different structural levels, follow different physical laws. Besides, the circular birefringence process also could lead to CPLE activity. Kuang et al reported the chiral self-assembled films from achiral CdSe/CdS nanorods by controlling the number of layers and angles between different layers. [100] The chiral film achieved the highest |*gCPLE*| of 0.0997 with ten layers and a 45° inter-angle, attributed to the birefringence and dichroism of the well-aligned CdSe/CdS nanorod layers.

The highest  $|g_{CPLE}|$  value of chiral inorganic nanomaterials are listed in **Table 1** (below). Most chiral semiconductor nanomaterials and single 1D, 2D, and quasi-2D perovskites display low  $|g_{CPLE}|$  values in the order of  $10^{-3}$ . The incorporation materials with strong PL into chiral photonic composites is an alternative approach to obtain relatively high  $|g_{CPLE}|$  values as high as  $10^{-1}$  with chemically similar materials. Although the actual mechanisms of CPLE have not been discussed or misinterpreted in many cases, chiral perovskite nanomaterials self-assembled into higher order structures with CPS-dominant CPLE show the highest optical asymmetry among all inorganic nanomaterials with  $|g_{CPLE}|$  as high as 1.6 (**Table 1**). The CPL intensity is important for the potential applications, therefore the amplification strategy needs to be developed, and researchers could be inspired by the relative work in small organic molecules. For example, Fuchter et al got 500-fold amplification of  $|g_{CPLE}|$  value of organic molecules based on Förster resonance energy transfer process [4]

Chiral nanocarbons with CPLE activity is expected to be another growth area but not due to record  $|g_{CPLE}|$  values. Their advantage is high biocompatibility with human, bacterial, and plant cells, [35, 101] which cannot be stated about perovskites. Similar advantage can also be found for cellulose-based CPS-dominant materials that can be self-assembled with a variety of emitters. We

expect more CPL- and CPS-dominant carbon nanomaterials with CPLE are likely to be engineered for biomedical applications.

CPLE-active nanomaterials have been incorporated in chiral photonic devices, [64],[63, 102-105] and this trend is expected to accelerate. Some examples include circularly-polarized microlasers, [106] circularly polarized light detectors [103, 108] and electro-CPLE-active LED devices, [107] Reduced-dimension perovskite used as photonic filters enabled a CPLE detector with the special advantage of elasticity. The optical response remains > 90 % after 100 bends. The chiral composites impart environmental robustness in these devices with the best example being a CPLE detector that could be kept in air for one month, showing no performance degradation. Recently, the first electro-CPLE-active LED devices has been developed with the achiral perovskite nanocrystals as the emitting layer and chiral perovskite (*R*-/*S*-MBA)<sub>2</sub>PbI<sub>4</sub> as the chiral layer. While the degree of polarization for emitted photons is now small (<3%), it is expected to increase by about an order of magnitude over the next ten years. The broader emergence and proliferation of electrically-pumped CPLE devices based on chiral nanostructures are envisioned.

**Acknowledgements:** We would like to thank Prof. Bin Li and Prof. Tianyong Zhang for helpful discussions with S. J. during the preparation of the manuscript. Financial support of this work for S.J. from the National Science Foundation of China (21908161), is gratefully acknowledged. N.AK. thanks the MURI Office of Naval Research (MURI N00014-20-1-2479); Vannevar Bush DoD Fellowship ONR N000141812876; ONR COVID-19 Newton Award "Pathways to Complexity with 'Imperfect' Nanoparticles' HQ00342010033 and AFOSR FA9550-20-1-0265, are gratefully acknowledged.

<b>Table 1.</b> Selected   <i>gCPLE</i>   values for chiral inorganic nanomaterials				
Category		Chiral unit	Highest  g_CPLE	Reference
CPL-dominant CPLE	Luminescent metallic nanoclusters	Chiral Ag <sub>29</sub> (R/S-DHLA) <sub>12</sub> nanoclusters	2×10 <sup>-3</sup>	28
	Nanocarbons	Sidewall of carbon nanotubes	1×10 <sup>-1</sup>	40
	Single semiconductor NPs	CdS NPs	8.0×10 <sup>-3</sup>	24
	Chiral Perovskites	CsPbBr <sub>3</sub> NPs	6.8×10 <sup>-2</sup>	61
		Lead-free 3- (fluoropyrrolidinium)MnBr <sub>3</sub>	$6.1 \times 10^{-3}$	79
CPS-dominant CPLE	Assembly of chiroplasmonic nanostructuress	Assemblies of AuAg nanoclusters	2.7×10 <sup>-2</sup>	33
	Superstructures with multiscale chirality	Assemblies of Au NPs	1 × 10 <sup>-2</sup>	16
	Assemblies on templates	Helical assembly of nanocarbons on helical fibers	$2 \times 10^{-3}$	74
	Chiral nanocomposites	PVA/CaCO <sub>3</sub> /CdTe helical fiber	$3.7 \times 10^{-3}$	86
		Chiral polyacetylene derivative and achiral fluorescent material	3.2×10 <sup>-1</sup>	87
	Cholesteric nanocomposite based on cellulose nanofibers.	Co-assembly of cellulose nanocrystals and ZnS/CdSe NPs	4.8× 10 <sup>-1</sup>	89
		Perovskites imbedded into chiral photonic nanocomposite	1.6	73

### References

- [1] L. Xiao, T. An, L. Wang, X. Xu, H. Sun, Nano Today 2020, 30, 100824.
- [2] G. Longhi, E. Castiglioni, J. Koshoubu, G. Mazzeo, S. Abbate, *Chirality* **2016**, *28*, 696.
- [3] F. Zinna, L. Di Bari, *Chirality* **2015**, *27*, 1.
- [4] J. Wade, J. R. Brandt, D. Reger, F. Zinna, K. Y. Amsharov, N. Jux, D. L. Andrews, M. J. Fuchter, *Angewandte Chemie* **2021**, *133*, 224.
- [5] N. A. Kotov, EPL (Europhysics Letters) 2017, 119, 66008.
- [6] D. W. Urry, J. Krivacic, *Proceedings of the National Academy of Sciences* **1970**, *65*, 845.
- [7] C. Bustamante, I. J. Tinoco, M. F. Maestre, Proc Natl Acad Sci USA 1983, 80, 3568.
- [8] M. A. van Dijk, A. L. Tchebotareva, M. Orrit, M. Lippitz, S. Berciaud, D. Lasne, L. Cognet, B. Lounis, *Phys. Chem. Chem. Phys.* **2006**, *8*, 3486.
- [9] C. Langhammer, B. Kasemo, I. Zorić, The Journal of Chemical Physics 2007, 126, 194702.
- [10] S. Yoo, Q. Park, Sci. Rep.-UK 2015, 5.
- [11] Z. Li, R. Zhao, T. Koschny, M. Kafesaki, K. B. Alici, E. Colak, H. Caglayan, E. Ozbay, C. M. Soukoulis, *Appl. Phys. Lett.* **2010**, *97*, 81901.
- [12] J. Dong, J. Li, *Progress In Electromagnetics Research* **2012**, *124*, 331.
- [13] S. Yoo, Q. Park, Opt. Express 2012, 20, 16480.
- [14] M. Xu, X. Wu, Y. Yang, C. Ma, W. Li, H. Yu, Z. Chen, J. Li, K. Zhang, S. Liu, ACS Nano 2020, 14, 11130.
- [15] H. Jiang, D. Qu, C. Zou, H. Zheng, Y. Xu, New J. Chem. 2019, 43, 6111.
- [16] H. Zheng, W. Li, W. Li, X. Wang, Z. Tang, S. X. Zhang, Y. Xu, Adv. Mater. 2018, 30, e1705948.
- [17] W. Jiang, Z. B. Qu, P. Kumar, D. Vecchio, Y. Wang, Y. Ma, J. H. Bahng, K. Bernardino, W. R. Gomes, F. M. Colombari, A. Lozada-Blanco, M. Veksler, E. Marino, A. Simon, C. Murray, S. R. Muniz, A. F. de Moura, N. A. Kotov, *Science* **2020**, *368*, 642.
- [18] B. Zhao, H. Yu, K. Pan, Z. Tan, J. Deng, ACS Nano 2020, 14, 3208.

- [19] L. Wang, K. W. Smith, S. Dominguez-Medina, N. Moody, J. M. Olson, H. Zhang, W. Chang, N. Kotov, S. Link, *ACS Photonics* **2015**, *2*, 1602.
- [20] Q. Zhang, T. Hernandez, K. W. Smith, S. A. Hosseini Jebeli, A. X. Dai, L. Warning, R. Baiyasi, L. A. McCarthy, H. Guo, D. Chen, J. A. Dionne, C. F. Landes, S. Link, *Science* **2019**, *365*, 1475.
- [21] J. T. Collins, K. R. Rusimova, D. C. Hooper, H. H. Jeong, L. Ohnoutek, F. Pradaux-Caggiano, T. Verbiest, D. R. Carbery, P. Fischer, V. K. Valev, *Phys. Rev. X* **2019**, *9*.
- [22] D. S. K. Y. Jamie L. Lunkley, J. Am. Chem. Soc. 2008.
- [23] G. Muller, Dalton Trans 2009, 9692.
- [24] R. Carr, N. H. Evans, D. Parker, Chem. Soc. Rev. 2012, 41, 7673.
- [25] M. Naito, K. Iwahori, A. Miura, M. Yamane, I. Yamashita, *Angew Chem Int Ed Engl* **2010**, 49, 7006.
- [26] T. Tomiyama, H. Yamazaki, Appl. Surf. Sci. 2017, 421, 831.
- [27] X. Kang, M. Zhu, Chem. Soc. Rev. 2019, 48, 2422.
- [28] A. C. Dharmaratne, T. Krick, A. Dass, J. Am. Chem. Soc. **2009**, 131, 13604.
- [29] J. Kumar, T. Kawai, T. Nakashima, Chem Commun (Camb) 2017, 53, 1269.
- [30] K. R. Krishnadas, L. Sementa, M. Medves, A. Fortunelli, M. Stener, A. Fürstenberg, G. Longhi, T. Bürgi, *ACS Nano* **2020**, *14*, 9687.
- [31] V. A. Sinani, P. Podsiadlo, J. Lee, N. A. Kotov, K. Kempa, *Int. J. Nanotechnol.* 2007, 4, 239.
- [32] J. Liu, P. N. Duchesne, M. Yu, X. Jiang, X. Ning, R. D. Vinluan, P. Zhang, J. Zheng, *Angewandte Chemie International Edition* **2016**, *55*, 8894.
- [33] L. Shi, L. Zhu, J. Guo, L. Zhang, Y. Shi, Y. Zhang, K. Hou, Y. Zheng, Y. Zhu, J. Lv, S. Liu, Z. Tang, *Angew Chem Int Ed Engl* **2017**, *56*, 15397.
- [34] Z. Suo, X. Hou, J. Chen, X. Liu, Y. Liu, F. Xing, Y. Chen, L. Feng, *Journal of physical chemistry*. C 2020, 124, 21094.
- [35] N. Suzuki, Y. Wang, P. Elvati, Z. B. Qu, K. Kim, S. Jiang, E. Baumeister, J. Lee, B. Yeom, J. H. Bahng, J. Lee, A. Violi, N. A. Kotov, *ACS Nano* **2016**, *10*, 1744.

- [36] A. Li, D. Zheng, M. Zhang, B. Wu, L. Zhu, *Langmuir* **2020**, *36*, 8965.
- [37] R. Malishev, E. Arad, S. K. Bhunia, S. Shaham-Niv, S. Kolusheva, E. Gazit, R. Jelinek, *Chem. Commun.* **2018**, *54*, 7762.
- [38] E. Arad, S. K. Bhunia, J. Jopp, S. Kolusheva, H. Rapaport, R. Jelinek, *Advanced Therapeutics* **2018**, *1*, 1800006.
- [39] J. Ahlawat, S. Masoudi Asil, G. Guillama Barroso, M. Nurunnabi, M. Narayan, *Biomater. Sci.-UK* **2021**, *9*, 626.
- [40] G. Ragazzon, A. Cadranel, E. V. Ushakova, Y. Wang, D. M. Guldi, A. L. Rogach, N. A. Kotov, M. Prato, *Chem* **2021**, *7*, 606.
- [41] J. Wang, G. Zhuang, M. Chen, D. Lu, Z. Li, Q. Huang, H. Jia, S. Cui, X. Shao, S. Yang, Du P, *Angew Chem Int Ed Engl* **2020**, *59*, 1619.
- [42] Y. Deng, M. Wang, Y. Zhuang, S. Liu, W. Huang, Q. Zhao, Light: Science & Applications 2021, 10.
- [43] Y. Sang, J. Han, T. Zhao, P. Duan, M. Liu, Adv. Mater. 2020, 32, 1900110.
- [44] J. E. Field, G. Muller, J. P. Riehl, D. Venkataraman, J. Am. Chem. Soc. 2003, 125, 11808.
- [45] N. Saleh, B. Moore, M. Srebro, N. Vanthuyne, L. Toupet, J. A. G. Williams, C. Roussel, K. K. Deol,
  G. Muller, J. Autschbach, J. Crassous, *Chemistry A European Journal* 2015, 21, 1673.
- [46] J. R. Brandt, X. Wang, Y. Yang, A. J. Campbell, M. J. Fuchter, J. Am. Chem. Soc. 2016, 138, 9743.
- [47] A. Ben-Moshe, A. Teitelboim, D. Oron, G. Markovich, Nano Lett. 2016, 16, 7467.
- [48] X. Shao, T. Zhang, B. Li, M. Zhou, X. Ma, J. Wang, S. Jiang, *Inorg. Chem.* **2019**, *58*, 6534.
- [49] T. Ni, D. K. Nagesha, J. Robles, N. F. Materer, S. Müssig, N. A. Kotov, *J. Am. Chem. Soc.* **2002**, 124, 3980.
- [50] X. Gao, X. Zhang, K. Deng, B. Han, L. Zhao, M. Wu, L. Shi, J. Lv, Z. Tang, J. Am. Chem. Soc. 2017, 139, 8734.
- [51] U. Tohgha, K. K. Deol, A. G. Porter, S. G. Bartko, J. K. Choi, B. M. Leonard, K. Varga, J. Kubelka,G. Muller, M. Balaz, ACS Nano 2013, 7, 11094.

- [52] J. Cheng, J. Hao, H. Liu, J. Li, J. Li, X. Zhu, X. Lin, K. Wang, T. He, ACS Nano 2018, 12, 5341.
- [53] J. Hao, Y. Li, J. Miao, R. Liu, J. Li, H. Liu, Q. Wang, H. Liu, M. Delville, T. He, K. Wang, X. Zhu, J. Cheng, ACS Nano 2020, 14, 10346.
- [54] J. Hao, F. Zhao, Q. Wang, J. Lin, P. Chen, J. Li, D. Zhang, M. Chen, P. Liu, M. H. Delville, T. He,J. Cheng, Y. Li, Adv. Opt. Mater. 2021, 2101142.
- [55] J. R. Poindexter, R. Hoye, L. Nienhaus, R. C. Kurchin, A. E. Morishige, E. E. Looney, A. Osherov, J. P. Correa-Baena, B. Lai, V. Bulovic, V. Stevanovic, M. G. Bawendi, T. Buonassisi, *ACS Nano* **2017**, *11*, 7101.
- [56] L. Theofylaktos, K. O. Kosmatos, E. Giannakaki, H. Kourti, D. Deligiannis, M. Konstantakou, T. Stergiopoulos, *Dalton Trans* **2019**, *48*, 9516.
- [57] D. G. Billing, A. Lemmerer, *Crystengcomm* **2006**, *8*, 686.
- [58] L. Mao, P. Guo, M. Kepenekian, I. Hadar, C. Katan, J. Even, R. D. Schaller, C. C. Stoumpos, M. G. Kanatzidis, *J. Am. Chem. Soc.* **2018**, *140*, 13078.
- [59] Y. Dong, Y. Zhang, X. Li, Y. Feng, H. Zhang, J. Xu, Small **2019**, 15, e1902237.
- [60] C. Yuan, X. Li, S. Semin, Y. Feng, T. Rasing, J. Xu, Nano Lett. 2018, 18, 5411.
- [61] T. He, J. Li, X. Li, C. Ren, Y. Luo, F. Zhao, R. Chen, X. Lin, J. Zhang, *Appl. Phys. Lett.* **2017**, *111*, 151102.
- [62] Y. H. Kim, Y. Zhai, E. A. Gaulding, S. N. Habisreutinger, T. Moot, B. A. Rosales, H. Lu, A. Hazarika, R. Brunecky, L. M. Wheeler, J. J. Berry, M. C. Beard, J. M. Luther, *ACS Nano* **2020**, *14*, 8816.
- [63] J. Ma, C. Fang, C. Chen, L. Jin, J. Wang, S. Wang, J. Tang, D. Li, ACS Nano **2019**, 13, 3659.
- [64] J. Wang, C. Fang, J. Ma, S. Wang, L. Jin, W. Li, D. Li, ACS Nano 2019, 13, 9473.
- [65] W. Chen, S. Zhang, M. Zhou, T. Zhao, X. Qin, X. Liu, M. Liu, P. Duan, J. Phys. Chem. Lett. 2019, 10, 3290.
- [66] X. Jin, M. Zhou, J. Han, B. Li, T. Zhang, S. Jiang, P. Duan, *Nano Res.* **2021**.
- [67] Y. Zhou, M. Yang, K. Sun, Z. Tang, N. A. Kotov, J. Am. Chem. Soc. **2010**, 132, 6006.

- [68] J. Yeom, U. S. Santos, M. Chekini, M. Cha, A. F. de Moura, N. A. Kotov, *Science* **2018**, *359*, 309.
- [69] A. Ben-Moshe, A. O. Govorov, G. Markovich, Angew Chem Int Ed Engl 2013, 52, 1275.
- [70] A. Ben-Moshe, S. G. Wolf, S. M. Bar, L. Houben, Z. Fan, A. O. Govorov, G. Markovich, *Nat. Commun.* **2014**, *5*, 4302.
- [71] J. Ahn, S. Ma, J. Y. Kim, J. Kyhm, W. Yang, J. A. Lim, N. A. Kotov, J. Moon, J. Am. Chem. Soc. 2020, 142, 4206.
- [72] Y. Dang, X. Liu, Y. Sun, J. Song, W. Hu, X. Tao, J. Phys. Chem. Lett. 2020, 11, 1689.
- [73] Y. Shi, P. Duan, S. Huo, Y. Li, M. Liu, Adv. Mater. 2018, 30, e1705011.
- [74] C. T. Wang, K. Chen, P. Xu, F. Yeung, H. S. Kwok, G. Li, Adv. Funct. Mater. 2019, 29, 1903155.
- [75] X. Yang, M. Zhou, Y. Wang, P. Duan, Adv. Mater. 2020, 32, e2000820.
- [76] S. Tsunega, R. H. Jin, T. Nakashima, T. Kawai, *ChemPlusChem* **2020**, 85, 619.
- [77] T. Sasaki, Y. Ida, I. Hisaki, S. Tsuzuki, N. Tohnai, G. Coquerel, H. Sato, M. Miyata, *Cryst. Growth Des.* **2016**, *16*, 1626.
- [78] J. T. Lin, D. G. Chen, L. S. Yang, T. C. Lin, Y. H. Liu, Y. C. Chao, P. T. Chou, C. W. Chiu, Angewandte Chemie 2021.
- [79] D. Di Nuzzo, L. Cui, J. L. Greenfield, B. Zhao, R. H. Friend, S. Meskers, ACS Nano 2020, 14, 7610.
- [80] J. X. Gao, W. Y. Zhang, Z. G. Wu, Y. X. Zheng, D. W. Fu, J. Am. Chem. Soc. 2020, 142, 4756.
- [81] H. Lu, C. Xiao, R. Song, T. Li, A. E. Maughan, A. Levin, R. Brunecky, J. J. Berry, D. B. Mitzi, V. Blum, M. C. Beard, *J. Am. Chem. Soc.* **2020**, *142*, 13030.
- [82] B. Sun, X. Liu, X. Li, Y. Zhang, X. Shao, D. Yang, H. Zhang, Chem. Mater. 2020, 32, 8914.
- [83] J. Wang, H. Zhou, J. Yang, L. Feng, J. Yao, K. Song, M. Zhou, S. Jin, G. Zhang, H. Yao, *J. Am. Chem. Soc.* **2021**, *143*, 10860.
- [84] Y. Duan, L. Han, J. Zhang, S. Asahina, Z. Huang, L. Shi, B. Wang, Y. Cao, Y. Yao, L. Ma, C. Wang, R. K. Dukor, L. Sun, C. Jiang, Z. Tang, L. A. Nafie, S. Che, *Angew Chem Int Ed Engl* **2015**, *54*, 15170.
- [85] Y. Kim, B. Yeom, O. Arteaga, S. Jo Yoo, S. Lee, J. Kim, N. A. Kotov, *Nat. Mater.* **2016**, *15*, 461.

- [86] G. Ragazzon, A. Cadranel, E. V. Ushakova, Y. Wang, D. M. Guldi, A. L. Rogach, N. A. Kotov, M. Prato, *Chem* **2021**, *7*, 606.
- [87] X. Jin, Y. Sang, Y. Shi, Y. Li, X. Zhu, P. Duan, M. Liu, ACS Nano 2019, 13, 2804.
- [88] Z. Tang, Science **2002**, 297, 237.
- [89] J. Zhang, W. Feng, H. Zhang, Z. Wang, H. A. Calcaterra, B. Yeom, P. A. Hu, N. A. Kotov, *Nat. Commun.* 2016, 7.
- [90] B. Zhao, X. Gao, K. Pan, J. Deng, ACS Nano 2021, 15, 7463.
- [91] K. P. A. J. Biao Zhao, *Macromolecules* **2018**.
- [92] M. Xu, C. Ma, J. Zhou, Y. Liu, X. Wu, S. Luo, W. Li, H. Yu, Y. Wang, Z. Chen, J. Li, S. Liu, *J. Mater. Chem. C* **2019**, *7*, 13794.
- [93] Y. Shi, Z. Zhou, X. Miao, Y. J. Liu, Q. Fan, K. Wang, D. Luo, X. W. Sun, *Journal of materials chemistry*. C, Materials for optical and electronic devices **2020**, 8, 1048.
- [94] H. Zheng, B. Ju, X. Wang, W. Wang, M. Li, Z. Tang, S. X. A. Zhang, Y. Xu, Adv. Opt. Mater. 2018, 6, 1801246.
- [95] J. He, K. Bian, N. Li, G. Piao, *Journal of materials chemistry. C, Materials for optical and electronic devices* **2019**, 7, 9278.
- [96] R. Xiong, S. Yu, M. J. Smith, J. Zhou, M. Krecker, L. Zhang, D. Nepal, T. J. Bunning, V. V. Tsukruk, *ACS Nano* **2019**, *13*, 9074.
- [97] W. Li, M. Xu, C. Ma, Y. Liu, J. Zhou, Z. Chen, Y. Wang, H. Yu, J. Li, S. Liu, *ACS Appl. Mater. Inter.* 2019, 11, 23512.
- [98] S. Zhao, Y. Yu, B. Zhang, P. Feng, C. Dang, M. Li, L. Zhao, L. Gao, Adv. Opt. Mater. 2021, 2100907.
- [99] Z. Li, H. Liu, F. Li, J. Zhao, Y. Wang, *Part. Part. Syst. Char.* **2020**, *37*, 2000008.
- [100] L. Chen, C. Hao, J. Cai, C. Chen, W. Ma, C. Xu, L. Xu, H. Kuang, *Angewandte Chemie International Edition* **2021**.
- [101] M. Zhang, L. Hu, H. Wang, Y. Song, Y. Liu, H. Li, M. Shao, H. Huang, Z. Kang, Nanoscale 2018,

10, 12734.

- [102] J. M. Abendroth, D. M. Stemer, B. P. Bloom, P. Roy, R. Naaman, D. H. Waldeck, P. S. Weiss, P. C. Mondal, ACS Nano 2019, 13, 4928.
- [103] C. Chen, L. Gao, W. Gao, C. Ge, Du X, Z. Li, Y. Yang, G. Niu, J. Tang, *Nat. Commun.* **2019**, *10*, 1927.
- [104] C. K. Yang, W. N. Chen, Y. T. Ding, J. Wang, Y. Rao, W. Q. Liao, Y. Y. Tang, P. F. Li, Z. X. Wang,R. G. Xiong, Adv. Mater. 2019, 31, e1808088.
- [105] Y. Liu, L. Collins, R. Proksch, S. Kim, B. R. Watson, B. Doughty, T. R. Calhoun, M. Ahmadi, A. V. Ievlev, S. Jesse, S. T. Retterer, A. Belianinov, K. Xiao, J. Huang, B. G. Sumpter, S. V. Kalinin, B. Hu, O. S. Ovchinnikova, *Nat. Mater.* 2018, *17*, 1013.
- [106] Z. Yuan, Y. Zhou, Z. Qiao, C. Eng Aik, W. Tu, X. Wu, Y. Chen, ACS Nano 2021, 15, 8965.
- [107] Y. Kim, Y. Zhai, H. Lu, X. Pan, C. Xiao, E. A. Gaulding, S. P. Harvey, J. J. Berry, Z. V. Vardeny, J. M. Luther, M. C. Beard, *Science* 2021, 371, 1129.
- [108] L. Wang, Y. Xue, M. Cui, Y. Huang, H. Xu, C. Qin, J. Yang, H. Dai, M. Yuan, *Angew Chem Int Ed Engl* **2020**, *59*, 6442.